



Annual Review of Fluid Mechanics

Fluid Dynamics of Squirmers and Ciliated Microorganisms

Takuji Ishikawa

Department of Biomedical Engineering, Tohoku University, Sendai, Japan;
email: t.ishikawa@tohoku.ac.jp

Annu. Rev. Fluid Mech. 2024. 56:95–121

The *Annual Review of Fluid Mechanics* is online at fluid.annualreviews.org

<https://doi.org/10.1146/annurev-fluid-121021-042929>

Copyright © 2024 by the author(s).
All rights reserved

Keywords

swimming, cilia, flagella, microorganism, microrobot

Abstract

The fluid dynamics of microswimmers has received attention from the fields of microbiology, microrobotics, and active matter. Microorganisms have evolved organelles termed cilia for propulsion through liquids. Each cilium periodically performs effective and recovery strokes, creating a metachronal wave as a whole and developing a propulsive force. One well-established mathematical model of ciliary swimming is the squirmer model, which focuses on surface squirming velocities. This model is also useful when studying active colloids and droplets. The squirmer model has been recently used to investigate the behaviors of microswimmers in complex environments, their collective dynamics, and the characteristics of active fluids. Efforts have also been made to broaden the range of applications beyond the assortment permitted by the squirmer model, which was established to specifically represent ciliary flow and incorporate biological features. The stress swimmer model imposes stresses above the cell body surface that enforce the no-slip condition. The ciliated swimmer model precisely reproduces the behaviors of each cilium that engages in mutual hydrodynamic interactions. Mathematical models have improved our understanding of various microbial phenomena, including cell–cell and cell–wall interactions and energetics. Here, I review recent advances in the hydrodynamics of ciliary swimming and then discuss future challenges.



1. INTRODUCTION

Cilia: hair-like organelles, which are abundant and short, with the same structure as flagella, which are long and sparse

Eukaryotic flagellum: whip-like organelle with distributed dynein molecular motors

Metachronal wave: a wave that propagates across the entire cilia due to the phase lag of adjacent ciliary strokes

“The role of the infinitely small in nature is infinitely large”; these are the words of Louis Pasteur (1822–1895), who is regarded as the founder of modern microbiology. Although microorganisms cannot be observed with the naked eye, they are broadly distributed worldwide and have extensive effects on human life (Ingraham & Ingraham 2003). In efforts to understand microbial physiology and function, many natural scientists have focused on motility and swimming (Jahn & Votta 1972, Brennen & Winet 1977, Pedley & Kessler 1992, Berg 2004, Lauga & Powers 2009, Guasto et al. 2012, Persat et al. 2015, Lauga 2016, Bees 2020). Fluid dynamics has important roles in various microbial phenomena, including oceanic red tides (Durham et al. 2009), symbiosis (Raina et al. 2019), and multicellularity (Goldstein 2015). These biological functions emerge in the interplay between cellular motility and the surrounding environment.

To swim freely in liquids, microorganisms have evolved organelles such as flagella and cilia (Khan & Scholey 2018). Eukaryotic flagella and cilia have a nearly identical structure: nine outer doublet microtubules and two central pairs of microtubules (i.e., 9 + 2 structure) (Figure 1d). The doublet microtubules are cross-linked by dynein molecular motors and can actively bend using the sliding forces generated by dynein (Fisch & Dupuis-Williams 2011). The distinction between flagella and cilia is not strict, but long and sparse organelles are considered flagella, whereas short and abundant organelles are considered cilia. Each cilium generates thrust by repeating effective and recovery strokes (Figure 1c); metachronal waves of ciliary strokes (Figure 1a) propagate on the cell surface (Brennen & Winet 1977) (Figure 1a). Microorganisms change their swimming directions and speeds by actively modulating the beating of cilia or flagella or by passively moving within their physical environment. The ability to change swimming direction in response to a

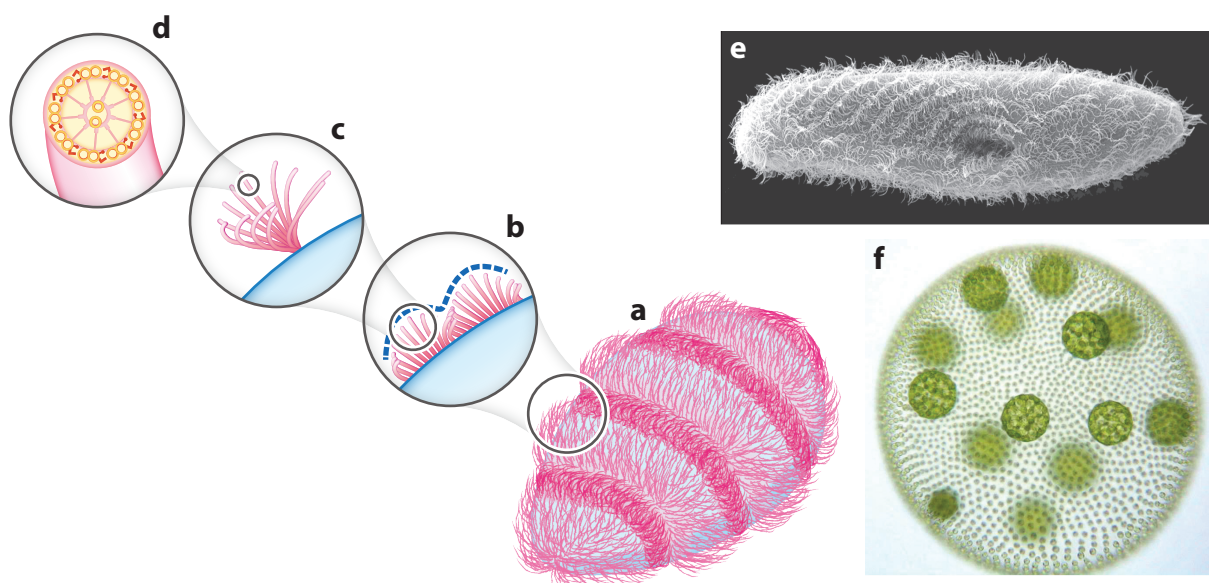


Figure 1

Hierarchical structure of ciliary movements. (a) Metachronal ciliary waves covering the body of a ciliate. (b) Coordinated ciliary movement creates the metachronal waves. (c) Each cilium performs an effective stroke and a recovery stroke. (d) Cross-section of a cilium showing the 9 + 2 structure and the dynein molecular motors that drive activity. (e) Scanning electron micrograph of *Paramecium caudatum*. Panel adapted with permission from Hausmann & Allen (2010). (f) Light appearance of *Volvox carteri*. Panel reproduced with permission from Aurora Nedelcu, University of New Brunswick.



physical stimulus is known as taxis; types of taxis include phototaxis in response to light, chemotaxis in response to a concentration field, gravitaxis in response to a gravity field, and rheotaxis in response to a flow field.

Ciliates are representative of microorganisms that possess cilia for swimming or crawling, as well as phagocytic food capture. Their habitats are diverse, including oceans, ponds, soil, fish gills, and mammalian digestive tracts. *Paramecium* spp. are well-known ciliates that have been the focus of many fluid dynamics studies. The body length and width of *Paramecium caudatum* (Figure 1e) are approximately 250 and 50 μm , respectively; approximately 15,000 cilia are distributed over the entire body of an individual organism, with a density of approximately 50 cilia per 100 μm^2 (Brennen & Winet 1977). The cilia are approximately 10–15 μm in length and 0.2 μm in diameter; they beat at a frequency of approximately 30 Hz. The organism swims approximately 10 body lengths per second. Other microorganisms that use cilia for swimming include volvocine green algae. *Volvox carteri* (Figure 1f) has a spherical body covered by approximately 4,000 cilia (Kirk 1998). The spherical shape of *V. carteri* is mathematically tractable; thus, it has been used as a model organism in studies of phototaxis, mass transport, the emergence of metachronal waves, and hydrodynamic interactions (Goldstein 2015). Many microorganisms also use cilia for swimming, and analysis of such swimming can increase the broader understanding of microbial physiology and function. In recent years, attempts have been made to artificially produce cilia (Milana et al. 2020, W. Wang et al. 2022). An understanding of ciliary flow and swimming also aids such efforts.

In 1952, M.J. Lighthill performed a mathematical analysis of ciliary swimming (Lighthill 1952). He focused on the surface created by the ciliary tips and assumed that the displacement and stretching of that surface could be expressed as a velocity boundary condition. This model with surface squirming velocities is what is now called a squirmer. The squirmer model has since been extended by Blake (1971) and Pedley et al. (2016) and used for various ciliary swimming analyses. In recent years, models aside from the squirmer model that more accurately reproduce ciliary flow and incorporate biological features have also been developed. To provide a thorough understanding of the mechanics of ciliary swimming, this review describes the fundamental hydrodynamics of ciliary swimming.

Section 2 first explains the hydrodynamics of microswimmers, which differ from the hydrodynamics of large swimmers because the effect of inertia is negligible and Stokes flow can be assumed. The relationship between forces exerted by flagella or cilia and the resulting swimming speeds is then discussed. Ciliary swimming as well as artificial self-propelled droplets and particles have been extensively analyzed with a squirmer model. Section 3 describes recent advances in squirmer hydrodynamics. Efforts have been made to broaden the range of applications beyond the squirmer model by representing ciliary flow in greater detail and incorporating biological features. Section 4 reviews studies using the stress swimmer model, which imposes stresses above the cell body. Section 5 reviews studies that use the ciliated swimmer model to precisely reproduce individual ciliary motion. Finally, current issues and future research prospects are discussed in Section 6.

2. HYDRODYNAMICS OF MICROSWIMMERS

2.1. Flow Around a Swimming Microorganism

The Reynolds number (Re) is a dimensionless number that describes flow conditions and indicates the ratio of inertial forces to viscous forces. It is defined as $\text{Re} = \rho UL/\mu$, where ρ is the fluid density, U is the swimming velocity, L is half of the body length, and μ is the fluid viscosity. The half body length of most microorganisms ranges from approximately 1 to 100 μm , and they swim at a speed of approximately 1 to 10 body lengths per second (Brennen & Winet 1977). The Re using density and viscosity of water ranges from $\text{Re} = 1 \times 10^{-5}$ to 1×10^{-1} . Therefore, the flow

Taxis: behavior of an organism toward a certain direction in response to a physical stimulus

Ciliate: a group of protists, alveolates, characterized by many short cilia arranged in rows

Algae: generic term of photosynthetic eukaryotic organisms that excludes mosses, ferns, and seed plants

Squirmer: microswimmer model with surface squirming velocity

Stokes flow: flow with negligible inertia, i.e., $\text{Re} \rightarrow 0$; also called creeping flow



Stresslet:

a force-dipole, consisting of two forces (thrust and drag) of the same magnitude and opposite direction placed on the same line

Bioconvection:

when microorganisms accumulate near the water surface, the upper region becomes denser than the lower region, creating overturning convection similar to Rayleigh–Bénard convection

field around a microorganism can be approximated as a Stokes flow; inertia can be neglected. Note, as a special case, that the effect of inertia may appear when large ciliates synchronize their ciliary strokes in escaping from an aggression (Hamel et al. 2011).

Stokes flow exhibits the unique properties of instantaneousness, reversibility, and superposition of solutions. Instantaneousness refers to when a microorganism stops the swimming apparatus (a flagellum or a cilium), and the surrounding flow instantaneously ceases and the microorganism does not move. Reversibility refers to when flagellar motion is reversed and the flow field and the velocity of a microorganism are also reversed. Thus, if the swimming apparatus simply beats back and forth, a microorganism oscillates in place. This is the Purcell scallop theorem (Purcell 1977). To move, flagella and cilia perform nonreciprocal effective and recovery strokes. The superposition of solutions can be attributed to the linearity of Stokes flow. Suppose that flow A is induced by external force A at one point in a fluid, whereas flow B is induced by external force B at another point. The flow induced by the simultaneous imposition of forces A and B is the sum of flows A and B. These basic properties of Stokes flow support an understanding of microbial swimming.

Another important property of Stokes flow is that the flow field induced by a force and higher moments of a cell's force distribution (e.g., a torque, a stresslet) can be analytically obtained by multiplying the moments by kernel functions called the propagators (Kim & Karrila 1991). Stresslet is a force-dipole, in which two forces of the same magnitude and opposite direction are placed along the same line. Stresslet is a first-order moment like torque, but torque induces an asymmetric stress tensor and stresslet induces a symmetric stress tensor. When the thrust forces exerted by flagella and cilia are known, the surrounding flow fields can be calculated by multiplying the kernel function by the thrust force.

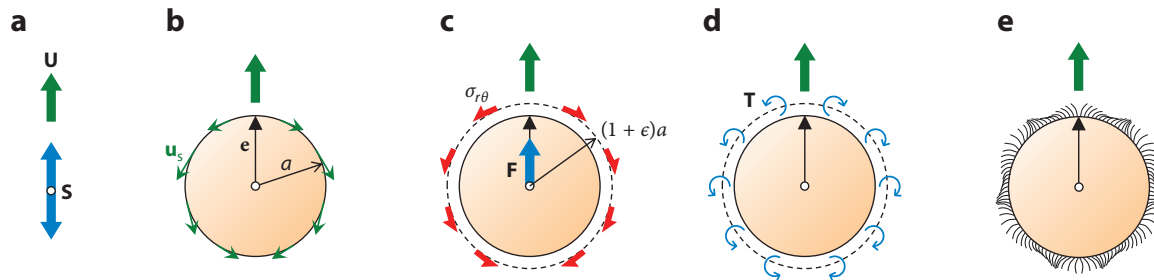
Microbial density may differ from ambient fluid density. When the sedimentation velocity caused by a density difference is much smaller than the swimming velocity, the density difference may be ignored. In this situation, the thrust and drag forces on the microorganism are in balance; the microorganism is force free (i.e., no external force acts on the microorganism). However, when sedimentation and swimming velocities are of the same order of magnitude (Drescher et al. 2009), or when discussing velocity fields far away from the microorganism (Drescher et al. 2010a), the effect of sedimentation cannot be ignored. Furthermore, in bioconvection, a convection phenomenon produced by microorganisms under gravity, the effects of sedimentation cannot be ignored (Hill & Pedley 2005, Bees 2020). In bioconvection, microorganisms that are denser than water accumulate near the water surface (because of taxis), leading to density instability that results in a descending plume.

The microbial center of gravity is not necessarily the geometric center; some microalgae, such as *V. carteri*, are bottom heavy (i.e., with a center of gravity behind the geometric center) (Drescher et al. 2009). This property causes the microorganisms to undergo external torque to orient vertically upward. By comparison, if a microorganism with asymmetric shape descends due to a density difference, the centers of gravity and drag may be misaligned, generating external torque (Roberts & Deacon 2002, Kage et al. 2020). This changes the microbial orientation to vertically upward or downward. For artificial microswimmers, external torque can be imparted by a magnetic force or other means to control the swimming direction.

2.2. Hydrodynamic Models of Ciliated Microswimmers

When an external force is applied to a microorganism, this induces flow in the surrounding fluid, and the disturbance velocity decays inversely proportional to the distance r . Moreover, the velocity induced by an external torque or a stresslet (force-dipole) decays at a rate dictated by r^{-2} . Higher-order moments decay more rapidly; the distant flow fields induced by microorganisms are dominated by external forces, torques, and stresslets. Figure 2e shows a spherical ciliated



**Figure 2**

Models of ciliated swimmers. (a) The point stresslet (force-dipole) model with stresslet \mathbf{S} and a prescribed swimming velocity \mathbf{U} . (b) A squirmer model with radius a and orientation \mathbf{e} , with the surface squirming velocities. (c) A stress swimmer model in which shear stress is applied to the fluid on a sphere of radius $(1 + \epsilon)a$; the fluid satisfies the no-slip condition on the spherical surface at radius a . (d) A torque swimmer model in which a torque is applied to the fluid on a sphere of radius $(1 + \epsilon)a$. (e) The ciliated swimmer model that precisely reproduces the behavior of each cilium.

swimmer such as the microalga *V. carteri*. In the absence of external forces and torques, the simplest hydrodynamic model of a ciliated swimmer is the point stresslet in **Figure 2a**. Because the point stresslet does not swim, the swimming velocity U is given additionally.

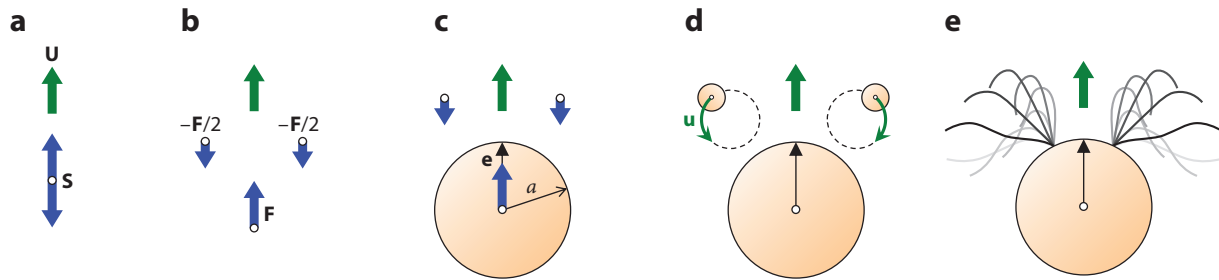
Between the ciliary swimming of **Figure 2e** and the point stresslet of **Figure 2a**, modeling at various resolutions is possible (**Figure 2b–d**). The model that comprehensively analyzes the motion of each cilium quantitatively evaluates the interactions between cilia and energy dissipation in the ciliary layer; however, it cannot manage a large number of swimmers owing to the large computational cost, and it is not applicable to other swimming bodies because of its excessive detail. In contrast, the simple point stresslet model is general in nature and can be applied to a wide range of swimmers; nevertheless, it does not consider the near-field hydrodynamic interactions nor the excluded volume effects and thus cannot be applied to highly concentrated suspensions or interactions between microbes and walls. No single hydrodynamic model is applicable to all problems; a model appropriate for the phenomenon of interest should be selected. In most cases, it is better to choose the minimal model that can describe the mechanism of the phenomenon of interest.

Figure 2b shows a squirmer model; the squirming velocity lies on the surface of a sphere of radius a . Although the body is not required to be spherical, we assume that it is for the sake of simplicity. When the surface created by the tips of all cilia is regarded as a body surface, a material point of that surface undergoes movement and stretching that can be expressed as a surface velocity. Thus, the body surface is represented by a velocity boundary that determines the swimming speed under specific force and torque conditions (for details, see Section 3).

In actual ciliary swimming, the cilia extending from the body move, but the shape of the body surface does not change. Therefore, the velocity on the body surface satisfies the no-slip condition. A cilium exerts a force on the fluid, and the reaction force is transmitted to the body as thrust. This thrust is balanced by the drag force. To model this mechanical condition, Ishikawa et al. (2020) developed a stress swimmer model; rather than imposing a squirming velocity on the surface, a shear stress was applied to the fluid on a sphere of radius $(1 + \epsilon)a$, where ϵa represents the ciliary length. The fluid must satisfy the no-slip condition on the spherical surface at radius a (**Figure 2c**). This model is useful when discussing cell–cell and cell–wall interactions because it approximately represents the flow in the ciliary layer (for details, see Section 4).

The force exerted by a cilium on fluid and the reaction force transmitted to the basal part of the cilium can be modeled as a torque. Ishikawa et al. (2016) developed a torque swimmer model;



**Figure 3**

Models of flagellated swimmers. (a) The point stresslet model with stresslet \mathbf{S} and a prescribed swimming velocity \mathbf{U} . (b) The multiple-point-force model with force \mathbf{F} and a prescribed swimming velocity. (c) The sphere and multiple-point-force model. The body has radius a and orientation \mathbf{e} . The swimming velocity is obtained under force-free conditions. (d) The multiple-sphere model in which flagellar beats are represented by the rotations of spheres. (e) The flagellated swimmer model that precisely reproduces the behavior of each flagellum.

a torque is applied to the fluid on a sphere of radius $(1 + \epsilon)a$ and the no-slip condition is applied to the body surface (**Figure 2d**). This model is useful when cells deform because the force-free condition can be strictly imposed with the torques (for details, see Section 4).

The ciliated swimmer model of **Figure 2e** precisely reproduces each cilium. Ito et al. (2019) used the waveform of each cilium to analyze swimming. This model calculates the hydrodynamic interactions among cilia and thus can treat energy dissipation within the ciliary layer. The drawback is that the computational cost is high (for details, see Section 5).

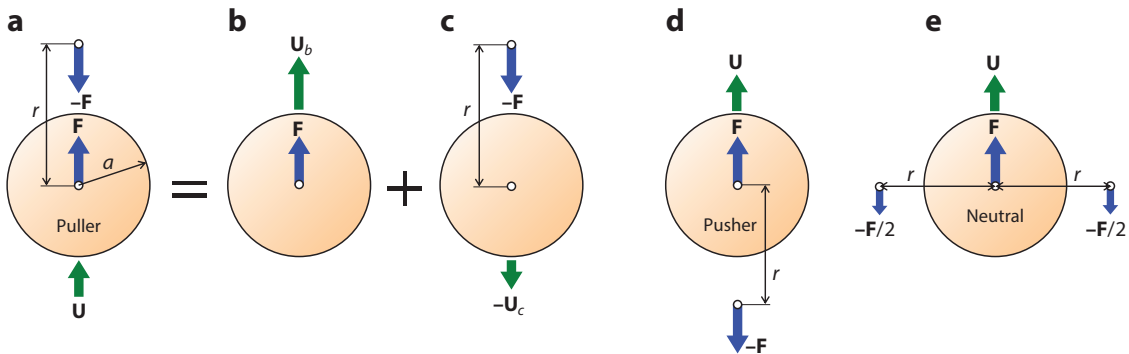
2.3. Hydrodynamic Models of Flagellated Microswimmers

Figure 3e shows an example of a flagellated swimmer, the microalga *Chlamydomonas*, that uses two flagella to move via the breaststroke. Several models have been developed that precisely reproduce the two flagellar waveforms. In the absence of external forces and torques, motion can be modeled as a simple point stresslet (**Figure 3a**), similar to the model for a ciliated swimmer. Between the flagellar swimming model of **Figure 3e** and the point stresslet model of **Figure 3a**, other models offer various resolutions (**Figure 3b-d**).

The flagellum produces a thrust force, whereas the cell produces a drag force. The multiple-point-force model of **Figure 3b** seeks to reproduce the points of action of the thrust and drag forces. Drescher et al. (2010a) used this model to express the time-averaged velocity field around *Chlamydomonas*. Ishimoto et al. (2017) reported that the unsteady velocity field around a human sperm could also be reproduced by varying the positions and magnitudes of the three forces over time. However, these models do not consider excluded volume effects, and the no-slip condition is not satisfied on the body surface.

The model in **Figure 3c**, which approximates the flagellum as a point force and models the cell body as a sphere, was used by Jibuti et al. (2014) to investigate the jet instability of concentrated *Chlamydomonas* suspensions. Maleprade et al. (2020) modeled the colonial alga *Gonium* by adding immobile thin rods to the disk-shaped body and imparting multiple flagellar forces. The thin rods mimic the flagellar drag when flagella stop beating. A model that represents the flagellar volume as a sphere and rotates the spheres with the flagellar beat frequency was proposed by Friedrich & Julicher (2012) (**Figure 3d**). By modeling the flagellum as a sphere, researchers can discuss the hydrodynamic interactions between flagella. Using this model, Brumley et al. (2012) reproduced the metachronal waves of *V. carteri*.



**Figure 4**

Force balances of the three types of microswimmers: a puller, a pusher, and a neutral swimmer. (a) The puller swimmer with radius a exhibits a propulsion apparatus in front of the body and exerts a point force $-F$ on the fluid at a distance r from the center of the sphere. The puller gains the thrust F as the reaction, and \mathbf{U} is the resultant swimming velocity. (b) A subproblem in which a force \mathbf{F} is exerted on a sphere. (c) A subproblem in which a point force $-F$ is exerted on the fluid at a distance r from the center of the sphere. (d) A pusher swimmer exhibits a propulsion apparatus behind the body and exerts a point force $-F$ on the fluid at a distance r from the center of the sphere. (e) A neutral swimmer exerts two point forces lateral to the body. The two forces possess magnitude $-F/2$ and are imparted at a distance r from the center of the sphere.

2.4. Flagellar Force During Free Swimming

Here, we comprehensively discuss flagellar thrust. For simplicity, consider a spherical microswimmer of radius a and density equal to the surrounding fluid density, which is freely swimming at velocity \mathbf{U} (Figure 4a). Suppose that the microswimmer exhibits a propulsion apparatus (such as a flagellum) in front of the body and exerts a point force $-F$ on the fluid at a distance r from the center of the sphere, where $r > a$. The microswimmer gains the thrust F as the reaction. Assume that Stokes flow is present around the microswimmer and that the thrust is balanced by the fluid drag (i.e., force free).

We derive the swimming velocity \mathbf{U} . Because Stokes flow permits superposition of solutions, the problem depicted in Figure 4a can be split into two subproblems (Figure 4b,c). In the subproblem depicted in Figure 4b, a thrust force \mathbf{F} is exerted on the sphere, and the sphere moves with velocity \mathbf{U}_b . According to Stokes law, the velocity is $\mathbf{U}_b = \mathbf{F}/(6\pi\mu a)$. The subproblem depicted in Figure 4c considers the motion of the sphere induced by the external point force $-F$ at the distance r . The sphere moves with velocity $-\mathbf{U}_c$ because of the flow field generated by the point force. The importance of the subproblem depicted in Figure 4c is sometimes ignored; however, this significantly affects actual swimming velocity. The velocity \mathbf{U}_c can be analytically derived (Kim & Karrila 1991), and the resultant swimming velocity \mathbf{U} is expressed as

$$\mathbf{U} = \mathbf{U}_b - \mathbf{U}_c = \frac{1}{6\pi\mu a} \left(1 - \frac{3a}{2r} + \frac{a^3}{2r^3} \right) \mathbf{F}. \quad 1.$$

When $r/a \rightarrow \infty$, the equation converges to Stokes law, i.e., $\mathbf{U} = \mathbf{U}_b = \mathbf{F}/(6\pi\mu a)$. When $\frac{r}{a} = 2$, $\mathbf{U} \cong 0.31 \mathbf{U}_b$, and approximately 70% of the thrust force does not contribute to propulsion. When $\frac{r}{a} = 1.1$ (reflecting the real cilia length), $\mathbf{U} \cong 0.012 \mathbf{U}_b$. Thus, approximately 99% of the thrust force does not contribute to propulsion. The distance r has a significant effect on the swimming velocity. If the cell body is fixed and the necessary force is measured, as described by Böddeker et al. (2020), the relationship between the force $-F$ exerted by the flagellum and the force f to be



measured is

Puller: propulsion apparatus in front of the body, as in microalgae *Chlamydomonas* spp.

Pusher: propulsion apparatus behind the body, as in *Escherichia coli* bacteria

The microswimmer of **Figure 4a** can be classified as a puller (the propulsion apparatus is in front of the body). When the propulsion apparatus is located behind the body, as in **Figure 4d**, the microswimmer is a pusher. Suppose that the pusher exerts a force $-\mathbf{F}$ on the fluid at a distance r from the center of the sphere (**Figure 4d**). Then, the swimming velocity \mathbf{U} of the pusher and puller are equivalent and can be determined with Equation 1.

When the centers of the thrust and drag forces are identical, the microswimmer is a neutral swimmer. For example, consider a spherical swimmer with two point forces imparted lateral to the body as shown in **Figure 4e**. Both forces possess magnitude $-F/2$ and lie at a distance r from the center of the sphere. The velocity of a sphere induced by a transverse point force can also be analytically derived (Kim & Karrila 1991). The swimming velocity \mathbf{U} of the neutral swimmer is

$$\mathbf{U} = \frac{1}{6\pi\mu a} \left(1 - \frac{3a}{4r} - \frac{a^3}{4r^3} \right) \mathbf{F}. \quad 3.$$

When $\frac{r}{a} = 1.1$, $\mathbf{U} \cong 0.13 \mathbf{U}_b$, and approximately 87% of the thrust force does not contribute to propulsion. The decrease in swimming velocity is smaller than the decrease represented by $\mathbf{U} \cong 0.012 \mathbf{U}_b$ for the puller and pusher because the flow generated by the transverse point forces is not directed toward the sphere.

To fully understand ciliary swimming, we must carefully consider the drag exerted on the swimmer by the cilia-generated flow (**Figure 4c**). Note that the linearity of Stokes flow allows for superposition of solutions. Accordingly, the effects of multiple forces can be superimposed. When the forces act diagonally, they can be separated into components parallel and perpendicular to the line connecting the point force and the center of the sphere; the forces can then be discussed separately. Additionally, although only translational motion is discussed in this section, analytical solutions are available for the torques induced by the point forces on the sphere (Kim & Karrila 1991). Thus, the rotational velocity of a microswimmer can also be derived.

3. BEHAVIORS OF SQUIRMERS

Studies using the squirmer model have been reviewed by Ishikawa (2009) and Pedley (2016). In this section, I summarize the basics of the model and review recent studies, published mainly after the review by Pedley (2016).

3.1. The Squirmer Model

The first model of a spherical squirmer was established by Lighthill (1952) and then extended by Blake (1971) and Pedley (2016). The extension of the squirmer to a spheroidal body shape was made by Keller & Wu (1977). Considering the envelope created by the tips of the cilia, a material point of the envelope surface undergoes movement and stretching; it can be expressed as a surface velocity. The radial, circumferential, and azimuthal surface velocities can be written as infinite series of Stokes equation eigenfunctions that describe arbitrary, time-dependent squirming velocities.

Although the original squirmer model imposed no restriction on surface velocity, many studies have assumed for simplicity that the surface velocity is steady, axisymmetric, and tangential to the surface. Furthermore, rather than using infinite series (Ghose & Adhikari 2014), only the first two squirming modes are considered because, for a solitary squirmer, the first mode defines the



swimming speed and the second mode defines the suspension viscosity. In this simple situation, the tangential surface velocity u_θ of the spherical squirmer is

$$u_\theta = \frac{3U_0}{2} (\sin\theta + \beta \sin\theta \cos\theta), \quad 4.$$

where U_0 is the swimming speed of the solitary squirmer and θ is the angle with the orientation vector \mathbf{e} . β is regarded as the squirmer parameter and constitutes the ratio of second-mode to first-mode squirming. A squirmer with a positive β is a puller; a squirmer with a negative β is a pusher. The actual microbial values of β are approximately 0.28 for *P. caudatum* (Ishikawa & Hota 2006) but very small for *V. carteri* (Short et al. 2006).

In recent years, artificial microswimmers have received considerable attention. The squirmer model has been useful, although it was originally developed for microorganisms. Some active colloids self-propel in aqueous media by generating local gradients of concentration or electric potential via surface reactions. During the mathematical analysis of phoretic microswimmers, the fluid domain is often split into two regions: the bulk region and the interfacial region around the particle (Moran & Posner 2017). Under the assumption that phoretic effects are confined to the thin interfacial region, such effects can be represented as surface slip velocities. Therefore, a phoretic microswimmer can be modeled as a squirmer. Some droplets also self-propel in aqueous media by generating Marangoni flow that can be attributed to interfacial energy gradients on the droplet interfaces (Seemann et al. 2016). Thutupalli et al. (2011) and Herminghaus et al. (2014) reported that the surface slip velocities of self-propelled droplets were similar to the velocity of a neutral squirmer with $\beta = 0$.

Squirmer parameter

β : the ratio of second-mode to first-mode squirming velocity in the infinite series of squirming velocities; positive β is a puller and negative β is a pusher

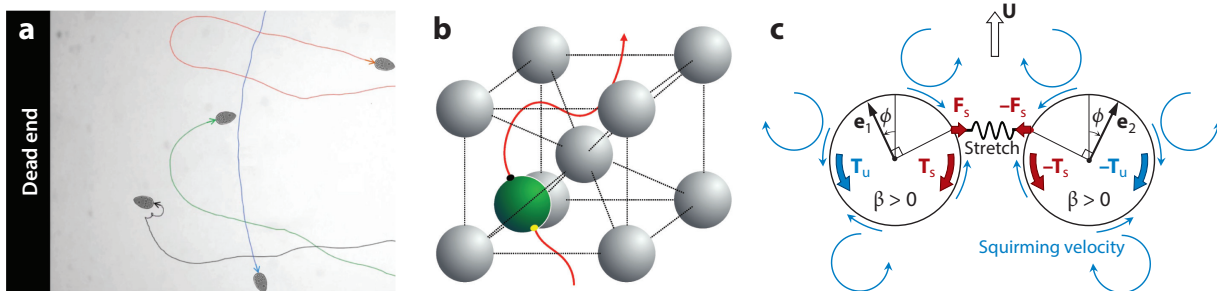
3.2. Behaviors Under Geometric Constraints

Microorganisms often live under geometric constraints, such as near a solid object, at a water surface, in granular matter, or in a porous medium. The behaviors of general microswimmers at interfaces were comprehensively described by Spagnolie & Lauga (2012). When a squirmer swims very close to a wall, a lubricating flow develops between the wall and the swimmer. The lubrication forces exerted on a squirmer in the vicinity of a solid wall, a rigid sphere, and a free surface are summarized by Ishikawa (2019b). All puller squirmers experience lubrication torques to swim away from a wall, regardless of the entry angle; strong pusher squirmers with $\beta \leq -2$ can be trapped by the lubrication torques, depending on the entry angle. The residence time on the wall surface increases monotonically according to the entry angle (Schaar et al. 2015). For a free surface, however, pusher squirmers experience lubrication torques to escape from the free surface, regardless of the entry angle; strong puller squirmers may be entrapped, depending on the entry angle. Overall, squirmer behaviors at solid walls and free surfaces differ considerably.

Squirmers behaviors at more complex interface geometries have also been reported: at a slip wall (Poddar et al. 2020), a fluid–fluid interface (Gidituri et al. 2022), and a deforming interface (Shaik & Ardekani 2017). Ishikawa & Kikuchi (2018) investigated squirmer behavior between two flat plates set at an acute angle. There was a dead-end line in the region of plate contact. Squirmers hydrodynamically escaped from that line, drawing symmetrical trajectories. A similar tendency in the ciliate *Tetrahymena thermophila* was observed (Figure 5a). The squirmer model explained the *Tetrahymena* escape mechanism, which involved lubrication torques exerted by the two walls.

Chamolly et al. (2017) modeled a porous medium as an infinite lattice of inert spheres and investigated the behaviors of a squirmer (Figure 5b). They observed four swimmer behaviors: straight trajectories, random walks, orbits, and stuck. Puller squirmers followed nearly straight paths through the lattice at nearly uniform speeds. Weak pusher squirmers were deflected by the inert spheres and thus performed random walks. When a pusher became stronger than



**Figure 5**

Behavior analyses of one or two squirmers. (a) Experiments with *Tetrabymena thermophila* seeking to avoid the dead end (squirmers behave similarly). The image is based on the work of Ishikawa & Kikuchi (2018). (b) A squirmer in an infinite lattice of inert spheres mimicking a porous medium. Panel adapted from Chamolly et al. (2017). (c) Stable side-by-side swimming of a dumbbell puller squirmer; hydrodynamic torque exerted by squirming velocity is balanced by the elastic torque of the spring. Panel adapted from Ishikawa (2019a).

approximately $\beta \leq -1.8$, a sharp transition to a trapped state was observed. A squirmer orbited a single inert sphere at small volume fractions, but it became stuck at larger volume fractions. Behavior was strongly influenced by the squirmer parameter and volume fraction.

Rheotaxis refers to the tendency of microorganisms to migrate in a certain direction relative to the background flow (Marcos et al. 2012, Kantsler et al. 2014). Rheotaxis by a spherical squirmer near a wall under shear flow was investigated by Uspal et al. (2015). For strong pullers with $\beta = 7$, rheotaxis developed because of the balance of torques induced by the squirming velocity and the background shear flow. Although puller squirmers generated lubrication torque to swim away from the wall (Ishikawa 2019b), strong pullers hydrodynamically returned to the wall and swam in a periodic manner (i.e., bouncing off the wall) (Li & Ardekani 2014). Ishimoto & Gaffney (2013) analyzed the swimming of not only spherical but also spheroidal squirmers and found a stable solution that allowed a strong puller squirmer to swim at a constant distance and angle from the wall. Through comprehensive studies of rheotaxis, Ishimoto (2017) explained the upstream (downstream) migration of a puller (pusher) squirmer by hydrodynamic interactions and interpreted the mechanism as similar to a weather vane, as the squirmer tail was directed downstream by the flow.

Rheotaxis is also evident in channel flow. Zöttl & Stark (2012) reported that squirmer rheotaxis emerged when thermal fluctuations were present; the squirmer moved in closed orbits in the absence of noise. A puller squirmer with thermal fluctuations in a Poiseuille flow gradually swam upstream along the centerline or was attracted to the tube wall, depending on its initial position and orientation. However, for pusher squirmers, all trajectories eventually converged to swinging motions around the centerline. Qi et al. (2020a) comprehensively studied this topic, and Dey et al. (2022) used self-propelling droplets to experimentally demonstrate such rheotaxis. Omori et al. (2022) showed that an unsteady microswimmer undergoing cyclic body deformation and variations in swimming velocity exhibited rheotaxis regardless of noise. The unsteady swimmer gradually became oriented against the channel flow and migrated to the channel center. The mechanism was mathematically explicable (Walker et al. 2022).

An understanding of microswimmer responses at walls might enable such motion to be controlled. Simmchen et al. (2016) prepared microscale steps that guided self-propelled, spherical Janus particles along edges over a long period. A simple squirmer model explained the mechanism involved. Dhar et al. (2020) numerically showed that the swimming directions of squirmers could be controlled by an appropriate wall geometry of a periodically tapered channel. Moreau &

Ishimoto (2021) used oscillatory background flow generated by an active wall for active squirmer control. Thus, geometric constraints significantly affect squirmer behavior.

3.3. Swimming in Complex Fluids

The physical environment inhabited by microorganisms is rich in variety, and the properties of the ambient fluid are also diverse. For example, temperature and concentration gradients often induce viscosity gradients. Datt & Elfring (2019) investigated squirmer behaviors in prescribed viscosity gradients. Squirmers swam straight in the absence of a viscosity gradient, but they turned toward regions of lower viscosity if a gradient was present. When the gradient was small, the rotational velocity vector Ω generated by the gradient was $\Omega = -\frac{1}{2\eta_0} \mathbf{U} \times \nabla \eta$, where \mathbf{U} is the velocity vector, η_0 is the mean viscosity, and $\nabla \eta$ is the viscosity gradient. Shaik & Elfring (2021) further explored the disturbance of the viscosity field caused by the squirmer. Regardless of the details of the disturbance, the squirmers tended to align down viscosity gradients, thus exhibiting negative viscotaxis. Another example is the density gradient of a pycnocline, which significantly affects squirmer swimming, energetics, and nutrient uptake (Doostmohammadi et al. 2012, Shaik & Ardekani 2021).

Fluids that become less viscous with increasing shear rate are known as shear-thinning fluids; examples include polymer solutions and blood, in which shear destroys the microstructures. Qiu et al. (2014) showed that a single-hinge microswimmer could self-propel in a shear-thinning fluid; the Purcell scallop theorem was no longer applicable. Squirmer behaviors in a shear-thinning fluid were investigated by Datt et al. (2015) using the Carreau–Yasuda model as the constitutive law. When shear-thinning was weak, the squirmer swam slower than in a Newtonian fluid, and the swimming velocity difference between a puller and a pusher disappeared. The swimming efficiency of a squirmer increased in shear-thinning fluids (Nganguia et al. 2017).

Fluids with elasticity are termed viscoelastic fluids. For example, in many biological fluids, the elastic forces in polymer chains elongated by flow ultimately return the polymers to their original lengths. Zhu et al. (2012) found that the squirmer swimming velocity was slower in a viscoelastic fluid than in a Newtonian fluid (similar to the findings in a shear-thinning fluid; see above). However, in contrast to a shear-thinning fluid, the pusher and puller swimming velocities differed in a viscoelastic fluid; the pusher swam more slowly when the elasticity was strong. Corato & D’Avino (2017) investigated the equilibrium orientation of a squirmer in a sheared viscoelastic fluid. Viscoelasticity caused the orientation vector to drift toward either the vorticity axis or the shear plane depending on viscoelastic strength; pullers and pushers had opposing equilibrium orientations. When a neutral squirmer swims in the Poiseuille flow of a viscoelastic fluid, swimming lift is exerted (Choudhary & Stark 2022). The swimming lift is two orders of magnitude stronger than the passive lift, thereby accelerating the centerline focusing of neutral squirmers.

Squirmers behaviors in a nematic liquid crystal have also been explored. Hydrodynamic coupling between the flow field around a squirmer and the liquid crystalline director led to squirmer reorientation (Lintuvuori et al. 2017). Soni et al. (2018) found that nematic liquid crystal activity significantly increased the squirmer swimming velocity. All the studies mentioned in this section illustrated that fluid rheological properties significantly influence squirmer swimming. In Stokes flow, inertia is negligible; the viscous effect is dominant and the constitutive equations governing rheological properties become important.

3.4. Hydrodynamics of a Squirmer Pair

Two-body interactions are important when exploring many-body interactions. The hydrodynamic interactions between two squirmers were comprehensively investigated by Ishikawa et al. (2006).



They used Faxén relationships to analyze far-field interactions, whereas near-field interactions were explored using lubrication theory. Further, the authors used a boundary element method to numerically calculate the intermediate regime. Squirmers coming into near contact exhibited substantial changes in orientation and eventually separated. Ishikawa et al. (2006) created a database of squirmer interactions, which enables the prediction of squirmer motions. Papavassiliou & Alexander (2017) derived exact solutions for the axisymmetric translation and rotation of a squirmer in the presence of a spherical or planar boundary. The results are valid at any separation (from near-field to far-field), though the exact motions in the perpendicular directions were not obtained.

Although lubrication theory states that two inert spheres cannot collide within a finite time, squirmers with surface slip velocities collide hydrodynamically (Potomkin et al. 2013). Jabbarzadeh & Fu (2018) showed that puller squirmers generate a feeding current that draws particles toward the swimmer, enabling them to approach target particles of any size. Therefore, when performing dynamic simulations of squirmers, short-range repulsive forces must be introduced to avoid squirmer collisions. The effect of the repulsive force on the two-body interaction of squirmers is not negligible when squirmers are in close proximity for long periods (Ishikawa 2022), but the effect is small for short-term collisions.

Darveniza et al. (2022) showed that lubrication theory combined with short-range repulsive forces reproduced the in-plane scattering of a pair of squirmers; the data were compared with the full numerical solutions. Dynamic scattering was divided into four categories: transient scattering, stationary binding, pairwise swimming, and circular orbiting. Theers et al. (2016) investigated the dynamic scattering of a pair of spheroidal squirmers in a narrow slit between two flat walls. There was a stable mode in which the two pullers could swim cooperatively in a wedge-like conformation with a small constant angle. The effects of inertia on two-squirmer interactions were discussed by Li et al. (2016) (up to a Re of 100). Inertial effects changed the scattering dynamics by inducing hydrodynamic attraction between two puller squirmers. More & Ardekani (2021) considered density stratification when exploring the effects of inertia and density on the interactions of two squirmers.

To generate stronger forces or enhance large-scale mixing, researchers have attempted to construct microswimmer assemblies (Wang et al. 2015). An understanding of the swimming behaviors and stability of a dumbbell squirmer is important when constructing a large assembly. A pair of puller squirmers connected by a spring achieved stable side-by-side swimming (Ishikawa 2019a) (**Figure 5c**); the squirming-induced hydrodynamic torque was balanced by the elastic torque of the spring. The swimming and transport of dumbbell squirmers were examined under thermal fluctuations (Clopés et al. 2020, 2022) and in a tube (Ouyang et al. 2022b). Large assemblies of squirmers, including a squirmer rod (Ouyang & Lin 2021) and a squirmer array (Ouyang et al. 2022a), have been analyzed in recent years. The findings will aid future design of microswimmer assemblies.

3.5. Collective Swimming

Chaotic active flow has been observed in suspensions of bacteria, sperm cells, and self-propelled colloids, despite the lack of inertia; this is known as active turbulence (Alert et al. 2022). The hydrodynamic interactions among self-propelled particles can create complex spatiotemporal flow structures (Koch & Subramanian 2011). Many continuum and discrete models have been used to explore the physical origin of chaotic active flow (Ishikawa 2009). Collective swimming of squirmers was first investigated by Ishikawa & Pedley (2008). In a monolayer setting, the squirmer aggregation, mesoscale spatiotemporal motion, and band formation could be attributed to purely hydrodynamic interactions.



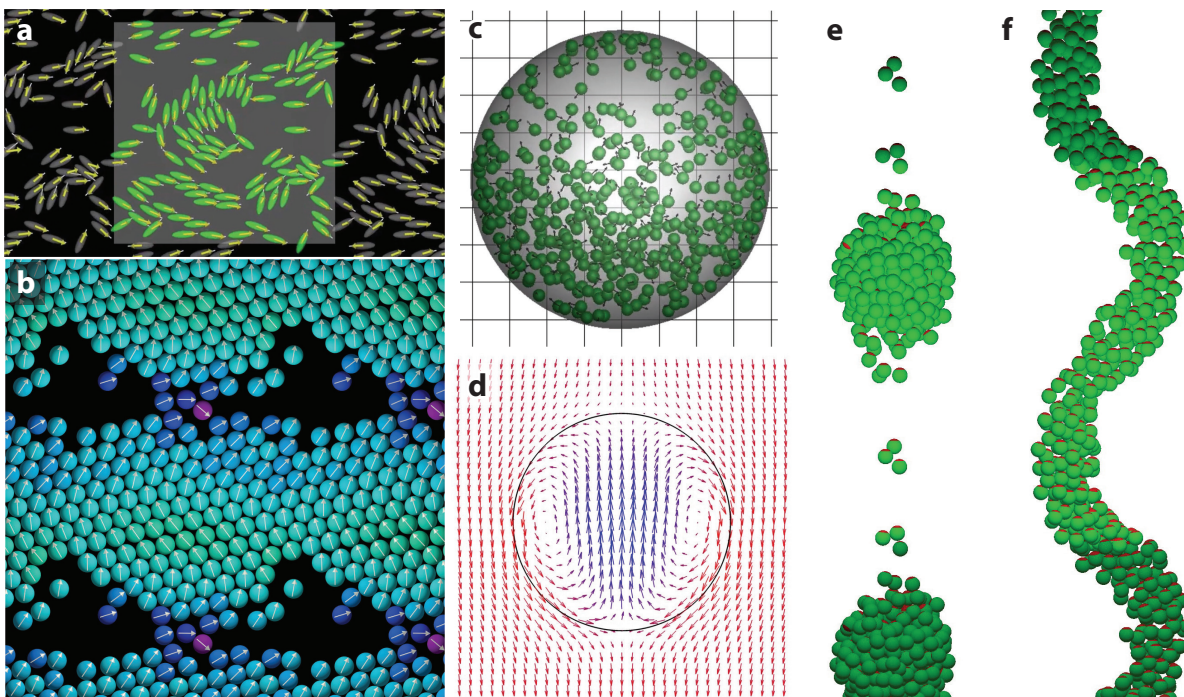


Figure 6

Collective behaviors of many squirmers. (a) Collective swimming of spheroidal pusher squirmers of $\beta = -0.3$ in a monolayer. Panel adapted from Kyoya et al. (2015). (b) A sheared concentrated suspension of squirmers used to explore rheological properties. Graphic is based on the work of Ishikawa et al. (2021a). (c,d) Active droplets driven by the collective motions of enclosed squirmers ($\beta = -3$) under gravity. Internal squirmers induce velocities on the droplet surface, and the entire droplet begins to exhibit single-squirmer behavior. Panels c and d adapted from Huang et al. (2020). (e,f) The instabilities of a jet of active fluid modeled using a suspension of squirmers. (e) For an active fluid of pullers, the jet breaks into droplets (similar to a Newtonian fluid). (f) For pushers, the jet buckles and exhibits waving instability. Panels e and f adapted from Ishikawa et al. (2022).

Kyoya et al. (2015) dynamically simulated spheroidal squirmers interacting hydrodynamically in a monolayer (Figure 6a). The near-field hydrodynamics played major roles in collective squirmer motion; the effects could be attributed to nearest-neighbor two-body interactions. Yoshinaga & Liverpool (2017) separated the contributions made by different length scales. During collective squirmer motion, lubrication forces and long-range hydrodynamic interactions were equally important. Brumley & Pedley (2019) showed that pairwise lubrication interactions combined with a short-range repulsive force reproduced the stable collective motions of squirmers. The importance of steric interactions was emphasized by Zantop & Stark (2022). Thus, near-field interactions play major roles in collective squirmer motion in concentrated suspensions.

For neutral squirmers, the orientational order is induced by hydrodynamic interactions (Ishikawa et al. 2008). Order stability is strongly affected by the squirmer parameter β and weakly affected by volume fraction (up to very high fractions) (Evans et al. 2011). By separating the contributions of different length scales, Yoshinaga & Liverpool (2018) found that the polar order was formed primarily by lubrication forces. Delfau et al. (2016) reported similar findings.

Notably, squirmer suspensions can exhibit phase separation. Zöttl & Stark (2014) analyzed squirmer suspensions in a slit bounded by two parallel walls. Phase separation could also be attributed solely to among-squirmer hydrodynamic interactions, although the equilibrium phase separation was commonly induced by attractive interparticle forces. A clear phase separation into



gaseous and clustered phases was observed for neutral squirmers, whereas a more gradual approach toward the cluster state was observed for strong pusher and puller squirmers. Theers et al. (2018) compared the phase separations of squirmers in the presence of active Brownian particles; the particles suppressed phase separation of spherical squirmers but enhanced phase separation of elongated squirmers.

Collective squirmer swimming is altered by geometric constraints. Shen & Lintuvuori (2019) investigated the behaviors of squirmers sedimented onto a flat wall. Although the squirming velocity was axisymmetric, the near-field hydrodynamic interactions induced the formation of rotating dimers or trimers (i.e., two or three squirmers bound together). Pusher squirmers created a stable polar order on a flat wall. Rühle & Stark (2020) introduced both top and bottom walls into a suspension of bottom-heavy squirmers that settled via gravity. Collections of sinking squirmers formed rolls and plumes reminiscent of bioconvection observed in earlier experiments (Hill & Pedley 2005, Bees 2020). Oyama et al. (2016) reported that a squirmer population formed a traveling wave between flat parallel walls. Thus, both collective and solitary squirmer swimming are strongly influenced by the physical environment.

3.6. Suspension Properties

A suspension of active particles exhibits unusual macroscopic rheological properties caused by microscale active stresses (Saintillan 2018). In a suspension of squirmers, both the particle stress Π^p and the normal viscous stress are present. The particle stress tensor and the stresslet \mathbf{S} exerted by an individual squirmer are related by the equation $\Pi^p = \frac{1}{V} \Sigma \mathbf{S}$; the stresslet is summed over the volume V (Batchelor 1970). The stresslet of a solitary squirmer in a fluid otherwise at rest is $\mathbf{S}_0 = 2\pi\mu a^2 U\beta(3\mathbf{e}\mathbf{e} - \mathbf{I})$, where \mathbf{e} is the orientation and \mathbf{I} is the identity tensor (Ishikawa et al. 2006). Thus, the rheological properties of a dilute squirmer suspension are governed by the squirmer orientation; an isotropic orientation is associated with zero particle stress and a polar order results in stresses that stretch or contract in the direction \mathbf{e} , depending on the sign of β . Ishikawa & Pedley (2007b) explored the rheology of semidilute squirmer suspensions. The shear viscosity of bottom-heavy puller (pusher) squirmers increased (decreased) in horizontal shear flow. When vertical shear flow was applied, this trend was reversed. The rheological properties in the concentrated regime were analyzed by Ishikawa et al. (2021a), who dynamically simulated a sheared monolayer suspension of squirmers (**Figure 6b**). For non-bottom-heavy squirmers, the shear viscosity increased more rapidly according to volume fraction compared with the shear viscosity of inert spheres. However, for bottom-heavy pusher squirmers, the viscosity could decrease even below the viscosity of the fluid phase. Thus, viscosity was strongly associated with the squirmer parameter β , bottom heaviness, and shear direction.

Swimming microorganisms facilitate mass transport in suspensions. Leptos et al. (2009) reported enhanced tracer diffusion in suspensions of *Chlamydomonas reinhardtii*; they also derived the short-term probability density functions (PDFs) of displacements involving Gaussian cores and robust exponential tails. Ortlieb et al. (2019) found that the long-term PDFs generated by *C. reinhardtii* became Gaussian; a squirmer model reproduced the PDFs. These trends were systematically described by Thiffeault (2015). In semidilute squirmer suspensions (Ishikawa et al. 2010) and in packed squirmer lattices (Kogure et al. 2023), tracer diffusion was significantly enhanced by swimming. The squirmer model adequately describes the mixing phenomena of larger organisms. Ouillon et al. (2020) measured effective diffusivity induced by the collective vertical migration of a swarm of *Artemia salina* (brine shrimp) through a stably stratified density interface. The squirmer model successfully explained the increase in effective diffusivity that could be attributed to swimming. Wang & Ardekani (2015) found that diapycnal eddy diffusivity was enhanced by squirmer activities in a regime of intermediate Re .



Self-diffusion in a suspension involves the diffusion of cells themselves rather than material diffusion. Translational squirmer self-diffusivity in a semidilute regime is inversely proportional to the squirmer volume fraction, whereas rotational squirmer self-diffusivity is proportional to the squirmer volume fraction (Ishikawa & Pedley 2007a). Rotational self-diffusivity is enhanced by more than one order of magnitude in polymer solutions (Qi et al. 2020b); this enhancement can be explained by asymmetrical encounters between polymers and squirmer surfaces, which create additional torque and random noise that can be attributed to rotational motion. Aragones et al. (2018) observed a significant increase in squirmer rotational diffusivity within a suspension of passive spheres; the squirmers trapped themselves in the suspension. Modica et al. (2022) measured the behavior of Janus particles in a porous medium; the translational diffusivities of active swimmers exhibited greater decreases compared with passive Brownian particles.

Active fluid:
a suspension of
self-propelled
particles, such as a
dense suspension of
bacteria

3.7. Active Fluids

An active fluid is a suspension of particles that can actively generate stress on the microscale (Zöttl & Stark 2016, Saintillan 2018). Kree et al. (2017) first analyzed the self-propulsion of spherical droplets of active fluid; internal active forces propelled the droplets. Kree et al. (2021) then showed that internal stresslets and quadrupoles could also induce self-propulsion of the active droplets. Huang et al. (2020) explored active droplets driven by the collective motion of enclosed squirmers under gravity (**Figure 6c**). The squirmers induced droplet migration in directions determined by the squirmer parameter β . Internal squirmers created velocities on droplet surfaces; the droplets then behaved as single squirmers (**Figure 6d**).

Ishikawa et al. (2022) investigated the instability of a jet of active fluid by considering a suspension of squirmers as an active fluid. The squirmers were assumed to be bottom heavy and heavier than the surrounding fluid, such that a downward jet self-assembled under gravity. The jets of active fluids were unstable; the instabilities of pullers and pushers differed. In an active fluid with pullers, the jet broke into droplets (similar to Plateau-Rayleigh instability of a Newtonian fluid) (**Figure 6e**). Kessler (1986) observed similar bulbous formation in experiments using *Chlamydomonas nivalis*. In an active fluid with pushers, by comparison, the jet buckled and exhibited waving instability (**Figure 6f**). The physical mechanisms involved were adequately explained on the basis of active stresses generated by squirmers. Studies of squirmer suspensions will broaden our understanding of the properties of active fluids.

4. STRESS AND TORQUE SWIMMERS

A ciliary swimming model different from the squirmer model has been proposed to more faithfully reproduce actual ciliary swimming and to incorporate biological features. The stress swimmer model imposes shear stresses on the fluid of a sphere of radius $(1 + \epsilon)a$, where ϵa represents the ciliary length (**Figure 2c**). The use of stresses (not velocities) is more realistic in modeling a ciliate, particularly when the microbes come close to each other or to a wall, because no slip is permitted on the body surface at $r = a$. On the other hand, the force exerted by a cilium on the fluid and the reaction force transmitted to the basal part of that cilium can be modeled as a torque. The torque swimmer model imposes torques on the fluid of a sphere of radius $(1 + \epsilon)a$ (**Figure 2d**). This model is useful when cells deform because it strictly applies the force-free condition under such circumstances.

4.1. Stress Swimmers

Active surfaces can be specified by using stresses rather than velocities. Keller et al. (1975) analyzed an ensemble of discrete forces exerted by cilia when creating a continuum distribution of



an unsteady force field. Short et al. (2006) modeled *V. carteri* as a rigid sphere with surface shear stress. The stress swimmer model with a shear stress shell over a no-slip body surface (**Figure 2c**) was used by Ohmura et al. (2018) and fully analyzed by Ishikawa et al. (2020). They derived the swimming speed U and rotation rate Ω of a neutrally buoyant stress swimmer in an infinite fluid otherwise at rest as

$$U = \frac{\pi\alpha}{6\mu} \left(\frac{4\alpha^3 - 3\alpha^2 - 1}{4\alpha} \right) f_\theta, \quad \Omega = -\frac{\pi}{8\mu} (\alpha^3 - 1) f_\phi, \quad 5.$$

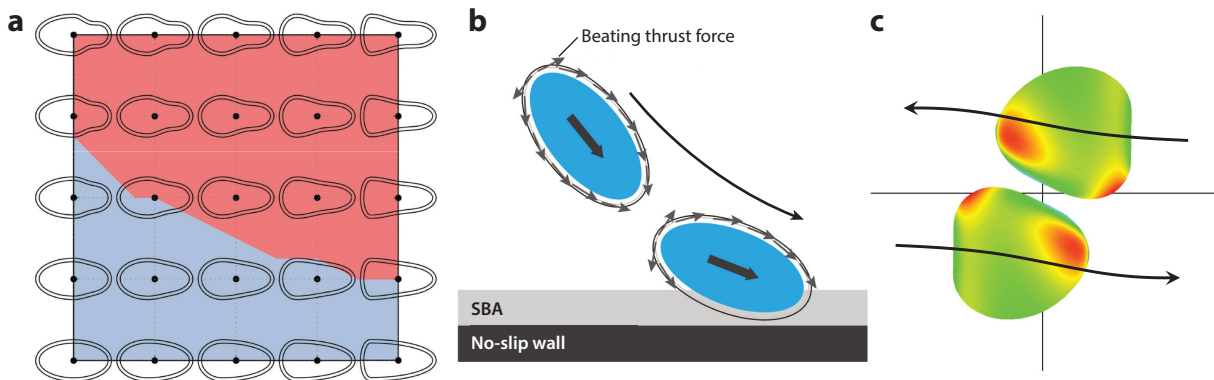
where $\alpha = 1 + \varepsilon$, and f_θ and f_ϕ are the shear stress components in the polar and azimuthal directions, respectively. When $\varepsilon \rightarrow 0$, both U and Ω asymptotically approach zero in proportion to ε . This tendency is equivalent to the tendency shown in Equation 3 for a spherical swimmer with two point forces applied lateral to the body (**Figure 4e**). The stress swimmer model explicitly represents the ciliary forces, as well as the viscous drag exerted on the body by ciliary flow.

Pairs of *V. carteri* colonies exhibit intriguing hydrodynamic bound states. When hovering under a top horizontal wall, the colonies are mutually attracted, such that they orbit each other in a waltz-like manner (Drescher et al. 2009). Ishikawa et al. (2020) used the stress swimmer model to simulate dancing *V. carteri*. The stress swimmer model was chosen because the squirmer model would generate a torque between the wall and the colony that is too large: The leading-order lubrication torque induced by the constant velocity surface increases as $\log(1/\xi)$, where ξ is the minimum distance between the wall and the velocity surface, whereas it is constant in the constant stress condition (Ishikawa 2019b). Hence, the waltzing motion of *V. carteri* was much more unstable in the squirmer model than in the experiment. To model the rotational swimming of *V. carteri*, Ishikawa et al. (2020) set the inclination angle in the direction of shear stress (relative to the colonial axis) to 15°. The two colonies hovering immediately below the top wall were mutually attracted by a flow that drew fluid in from the side and ejected it downward. The waltzing motion developed because the bottom-heaviness-induced torque that turned the organisms upward was balanced by the hydrodynamic-interaction-induced torque that forced the change in direction, resulting in orbital rotation at a tilted angle. In contrast, at the bottom of the container, *V. carteri* colonies oscillated horizontally back and forth in a minuet-like manner (Drescher et al. 2009). This bound state was also reproduced by the stress swimmer model (Ishikawa et al. 2020).

Ferracci et al. (2013) reported that the ciliate *T. thermophila* was hydrodynamically entrapped at a water-air interface but could escape from a solid wall. To clarify the entrapment phenomenon, Manabe et al. (2020) used the stress swimmer model to investigate behaviors at a water-air interface and a solid wall. Two major shape parameters dominated the entrapment phenomenon: fore-and-aft asymmetry and constriction (**Figure 7a**). When the stress swimmer exhibited a small amount of negative curvature, it was trapped by the water-air interface but escaped from a solid wall, consistent with experimental observations. Entrapment was explained by the balance between two opposing rotational velocities: a repulsive velocity that could be attributed to the ciliary beat and an attractive velocity that reflected collision at the interface.

In contrast, *Tetrahymena pyriformis* cells could reside on, and slide along, a solid wall by lowering the beat frequencies of cilia only in the vicinity of the wall (Ohmura et al. 2018). A similar sliding motion was observed in *P. caudatum* (Nishigami et al. 2018). Ohmura et al. (2018) used the stress swimmer model to model the reduction in ciliary beat frequency of *T. pyriformis* by lowering shear stress only near the wall (**Figure 7b**). An advantage of the stress swimmer model is its inclusion of one-to-one correspondence between ciliary motion and stress boundary conditions. The model reproduced the sliding phenomenon; asymmetric ciliary activity directed the torque toward the wall. Thus, the ciliate accumulated on surfaces (Okuyama et al. 2021). Ohmura et al. (2021) further subjected *T. pyriformis* to background shear flow. *T. pyriformis* exhibited positive



**Figure 7**

Behavioral analysis of stress and torque swimmers. (a) State diagram of the behaviors of stress swimmers of various shapes at a water–air interface, in which cell shapes are drawn for reference. The horizontal axis represents the strength of fore-and-aft asymmetry and the vertical axis represents the strength of negative curvature. Red regions indicate trapped cells; blue regions indicate escaped cells. Panel adapted from Manabe et al. (2020). (b) The sliding motion of a stress swimmer that lowers the shear stress only near the wall. Panel adapted from Ohmura et al. (2018). (c) Face-to-face interaction of deformable torque swimmers. Red regions experience high membrane tension. Panel adapted from Matsui et al. (2020a). Abbreviation: SBA, stop beating area.

rheotaxis at the wall and tended to swim upstream against the flow. Such rheotaxis was also reproduced by the stress swimmer model. The rheotaxis was explained by the presence of both a torque toward the wall (attributed to asymmetric ciliary motion) and an upstream torque (caused by shear flow), which constitute a mechanism similar to a weather vane. These findings illustrate the utility of stress swimmer models when analyzing the behaviors of ciliates near interfaces.

4.2. Torque Swimmers

Deformation of the ciliate *T. thermophila* swimming between flat walls was studied by Ishikawa & Kikuchi (2018). The body width increased by approximately 10% when cells avoided the dead end. Deformation of microswimmers in active droplets (Nagai et al. 2005, Tarama 2017) and during amoeboid swimming (Farutin et al. 2013, Morita et al. 2018) has also been reported. To explicitly account for the effects of body deformation, Ishikawa et al. (2016) developed a deformable torque swimmer model; the cell body was modeled as a capsule with a hyperelastic membrane and ciliary and reaction forces were modeled as a torque. Thus, even when the body is largely deformed, the force-free condition is strictly maintained. Furthermore, the torque swimmer model explicitly manages cell membrane deformation; the tension on the membranes can be calculated. Because the avoidance reaction of *Paramecium* spp. is induced by the opening of cell membrane calcium ion channels via mechanical stimuli (Naitoh & Eckert 1969), membrane tension is an important factor.

Ishikawa et al. (2016) investigated the deformation and swimming of torque swimmers. When the deformation was small, the membrane tension was larger at the anterior end than at the posterior end. However, when the deformation was large, the swimmer deformed to a heart-like shape, and the membrane tension was larger at the posterior end. Matsui et al. (2020b) investigated the behavior of deformable torque swimmers in shear flow. The swimmers tended to gradually become oriented toward the shear plane or the vorticity axis depending on dipole strength. Pullers were oriented toward the shear plane, whereas pushers were oriented toward the vorticity axis. Notably, a similar change in orientation was observed for a rigid squirmer swimming in a sheared viscoelastic fluid (Corato & D’Avino 2017). Thus, making the swimmer



itself elastic and making the surrounding fluid elastic are expected to produce similar swimmer behavior. Matsui et al. (2020b) analyzed the rheology of a dilute suspension of deformable torque swimmers. The apparent shear viscosity exhibited shear-thinning properties; the first normal stress difference had a positive sign. These rheological properties were explained by deformation and the direction of the swimmer's stresslet.

Matsui et al. (2020a) explored two-body interactions of deformable torque swimmers. During face-to-face interactions, deformation was particularly noticeable in the near-contact region. The anterior membrane tension was high when the two swimmers were in close proximity (**Figure 7c**) because of high pressure between the two near-contact surfaces. The nature of the strong stress considerably varied according to collision configuration; even when the configuration was the same, the location of strong stress considerably varied over time. When chasing each other, swimmers were mutually attracted; this phenomenon is not observed in velocity squirmer models. The torque swimmer model has been successful for discussing cellular deformation.

5. CILIATED SWIMMERS

Thus far, we have regarded ciliary force and velocity as continuous quantities, although cilia are discrete. The phases of individual ciliary beats do not exactly match; metachronal waves of beats propagate to the body surface. If the direction of beating is identical (opposite) to the direction of wave propagation, the metachronal wave is considered symplectic (antiplectic); if the direction of beating is to the right (left) relative to the wave, the wave is considered dexioplectic (laeoplectic) (Sleigh 1962). Ciliary flow has been extensively analyzed; both the envelope model, which concerns surface movement and deformation produced by the ciliary tips, and the sublayer model, which considers each cilium to be discrete, have long histories (Brennen & Winet 1977).

The intriguing mechanism by which metachronal waves emerge has been intensively studied (Gilpin et al. 2020). Brumley et al. (2014) performed sophisticated experiments; they observed two micropipette-held somatic cells of *V. carteri* with a high-speed camera while the separation distance was controlled. Close spacing induced robust synchrony over thousands of beats; the flagella were coupled only via fluid. Wan & Goldstein (2016) observed that the flagella of a *Chlamydomonas* mutant without filamentous connections between basal bodies exhibited a form of synchronization that significantly differed from wild-type synchronization. Thus, in addition to hydrodynamic coupling, intracellular structures facilitate flagellar synchronization by unicellular microorganisms. Several large-scale numerical simulations of planar ciliary arrays have appeared, revealing that metachronal waves can form via hydrodynamic interactions alone and that antiplectic metachronal waves are most efficient (Osterman & Vilfan 2011, Elgeti & Gompper 2013, Brumley et al. 2015).

The metachronal waves of ciliates form on a closed curved surface rather than on a flat surface, and they are continuously exposed to the bulk flow associated with swimming. When the metachronal waves of ciliates are being modeled, spatiotemporal variations in surface velocity can be added to the squirmer model; alternatively, spatiotemporal variations in stress can be added to the stress swimmer model. However, these models assume continuous ciliary activity; the models do not adequately manage hydrodynamic interactions between cilia or the energetics of the ciliary layer. To overcome this problem, Ito et al. (2019) developed a ciliated swimmer model by discretely placing hundreds of cilia on the surface of a sphere and then imposing a force-free condition during swimming (**Figure 8a**). Although their model is computationally demanding, it accurately represents flow within the ciliary layer, as well as the hydrodynamic interactions between each cilium and the surrounding flow during free swimming.

The time-averaged swimming speed of ciliated swimmers is substantially affected by the direction of the metachronal wave (Ito et al. 2019). An antiplectic wave with a wavenumber of



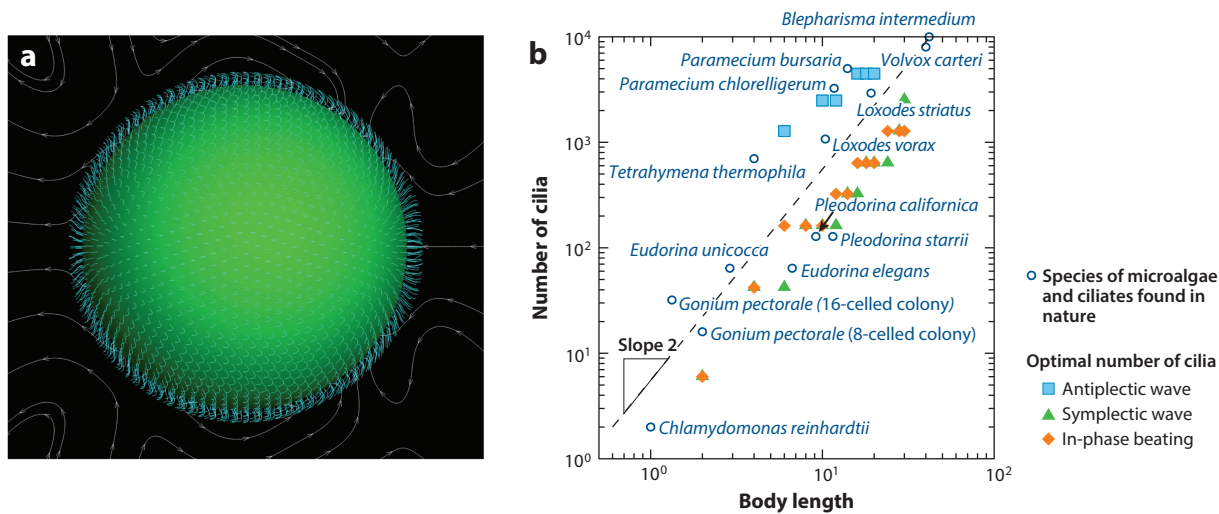


Figure 8

Ciliary swimming. (a) Flow field around a ciliated swimmer with approximately 1,000 cilia. Graphic based on the work of Ito et al. (2019) and provided by Dr. T. Omori (Tohoku University, Japan). (b) Number of cilia as a function of body length; the optimal number of cilia (filled symbols) increases at a slope of 2, which coincides with species of microalgae and ciliates found in nature (open circles). Panel adapted from Omori et al. (2020).

approximately 1 is associated with the fastest swimming speed, which is approximately threefold greater than the speed associated with a symplectic wave. This phenomenon occurs because the distance between the fore and the aft cilia during the effective strokes is greater for the antiplectic wave than for the symplectic wave; fluid flows more freely in the ciliary layer. The finding that antiplectic waves are most efficient is consistent with previous studies regarding ciliary carpets. Ito et al. (2019) found that more than 90% of energy was dissipated within the ciliary layer, considering strong shear induced by beating cilia. However, outside the ciliary layer, the conditions are adequately represented by the squirmer model. Therefore, the choice of using the ciliated swimmer model or the squirmer model should be based on whether the analysis considers the internal flow of the ciliary layer.

Omori et al. (2020) comprehensively explored scaling of ciliated swimmers. Considering the multicellularity of volvocine green algae, scaling proceeded by varying ciliary number and body radii; the ciliary length was maintained at a constant value. For both antiplectic and symplectic metachronal waves, the model yielded optimal ciliary number densities that maximized propulsive efficiency regardless of body radius. The propulsion efficiency of optimally ciliated swimmers decreased in an inverse manner, in proportion to the radius. If it is assumed that nutrient uptake increases according to the square of the radius, a larger body size may aid survival because the increase in uptake outweighs the decrease in swimming efficiency. The estimated optimal ciliary densities were consistent with the actual densities of ciliates and microalgae (Figure 8b). Thus, extant motile ciliates and microalgae may have survived by acquiring the optimal propulsion efficiency. The ciliated swimmer model has also been used to investigate the coordinated motion of cilia on a sphere (Westwood & Keaveny 2021) and during helical swimming (Rode et al. 2021).

6. PROSPECTS AND FUTURE DIRECTIONS

We have presented four models of ciliary swimming: squirmer, stress swimmer, torque swimmer, and ciliated swimmer. Each model has advantages and disadvantages. The squirmer model



is mathematically simple and widely applicable; velocity on the body surface is the only boundary condition of the flow field. The squirming velocity can include tangential and radial components, azimuthal swirling, and unsteady components (Pedley 2016). Furthermore, the model can be extended to nonspherical body shapes (van Gogh et al. 2022). Squirmers are thus widely used to represent ciliated microorganisms, as well as self-propelled droplets and particles. However, the model is unable to manage flow within the ciliary layer or explicitly represent ciliary forces. In contrast, the stress swimmer model explicitly represents ciliary forces and approximates ciliary flow by imposing a no-slip condition on the body surface. The disadvantage of the model is its imposition of a shear stress boundary on another surface, in addition to the velocity boundary on the body surface; the presence of this boundary complicates the mathematical assessment and increases the computational load. The advantages of the torque swimmer model include the advantages of the stress swimmer model, as well as its ability to represent body deformations. However, such deformation analysis involves solving new governing equations for the solid mechanics of the membrane, which makes the numerical code more complex and increases the computational load. The advantage of the ciliated swimmer model is that it represents the motion of each cilium and thus rigorously describes the hydrodynamics of ciliary swimming; however, this model has a large computational load. No single hydrodynamic model can solve all problems; there is a need to select the best model for each problem.

The broader hydrodynamic understanding of ciliary swimming has considerably increased over the past 50 years, but modeling of the biological response remains in the early stages. The phototaxis of microalgae *Volvox* (Drescher et al. 2010b) and *Gonium* (Maleprade et al. 2020) colonies was modeled in terms of the responses of individual cells to light. A reduction in the ciliary beat frequency of light-stimulated cells caused the entire colony to turn toward the direction of the light. However, it is unclear how phototaxis is controlled in other species. Gravitaxis can be caused by both bottom heaviness (Drescher et al. 2009) and shape asymmetry (Roberts & Deacon 2002). Some microalgae exhibit diel vertical migration; they swim toward the sea surface before dawn but move deeper at dusk (Shikata et al. 2015). They begin the ascent to the sea surface before the sky brightens, suggesting that phototaxis is not involved; it is unclear how such organisms control phototaxis and gravitaxis. Future research should explore the possibility of an internal clock. Because diel vertical migration is closely related to the onset of oceanic red tides, mathematical modeling and hydrodynamic experiments are necessary. The ciliary responses to flow fields are unknown and further research is essential.

Although the internal ciliary ultrastructure has been elucidated, the mechanisms by which dynein molecular motors power three-dimensional ciliary movements remain unclear (Ishikawa et al. 2021b). In particular, there is uncertainty regarding the mechanisms by which dynein is activated and inhibited to control waveform and frequency. The mechanisms are important to reproduce the responses of ciliary movements to physical stimuli. Narematsu et al. (2015) pointed out that ciliary basal structure is as important as hydrodynamics in the emergence of metachronal waves on *Paramecium* spp. Similar observations for the unicellular organism *C. reinhardtii* have been made (Wan & Goldstein 2016). The influence of the ciliary basal structure needs to be further investigated.

The ciliate *Paramecium*, for example, exhibits avoidance when stimulated on the anterior side and escape when stimulated on the posterior side (Naitoh & Eckert 1969). These responses are evident when cells collide with walls or other cells (Ishikawa & Hota 2006), but the responses are not extensively modeled. Notably, Kunita et al. (2016) explored memory in the ciliate *Tetrahymena*. Cells were briefly trapped in a small droplet of water and thus forced to follow a small circular trajectory. Upon release, the cells continued to travel in this trajectory. One possibility is that *Tetrahymena* remembers these changes by altering its body shape and ciliary movements



in response to small circular orbits. Another ciliate, *Stentor coeruleus*, can recognize the shape of the surrounding space and adhere to a narrow area (Echigoya et al. 2022). Because microorganisms exhibit a great range of responses and unexpected behaviors in response to environmental changes, many discoveries are expected.

When considering large-scale microbial phenomena (e.g., oceanic red tides and bioreactors), it is essential to mathematically reduce cellular phenomena to the macroscale, as demonstrated by Pedley & Kessler (1992) and Bees (2020). There is a continuing effort by researchers to build a continuum model using a cellular activity database (Ishikawa 2012). The applications of such research must be expanded to environmental studies, medicine, and engineering. Microrobotics research is rapidly proceeding with respect to artificial cilia and self-propelled particles (Moran & Posner 2017, Milana et al. 2020, L. Wang et al. 2021, W. Wang et al. 2022). The studies introduced in this review enhance our understanding of flow and swimming in artificial systems. I hope that this review aids future research focused on swimming microorganisms and microswimmers.

SUMMARY POINTS

1. When cilia length is shorter than the body length, the flow created by the cilia strongly interferes with the body surface, causing resistance. Therefore, only a small fraction of the force exerted by the cilia on the fluid contributes to propulsion.
2. Models of ciliary swimming at different resolutions, from a point stresslet to a ciliated swimmer, are available. No single hydrodynamic model is applicable to all problems; a minimal model appropriate for the phenomenon of interest should be selected.
3. Squirmer models have been used to analyze microorganisms and self-propelled particles, helping to elucidate various phenomena, such as collective swimming and active fluid properties.
4. Ciliates change their flagellar beat or deform their bodies in response to physical stimuli. Models that take into account these biological characteristics have been proposed.
5. Most of the mechanical energy consumed in ciliary swimming is dissipated within the ciliary layer. The ciliated swimmer model allows for discussion of the energy of ciliary swimming.

FUTURE ISSUES

1. The mechanisms of biological responses of microorganisms to physical stimuli are not well understood, and these need to be clarified and mathematically modeled in the future.
2. The regulatory mechanism of the dynein motors in the ciliary axoneme is not yet clear. A mechanical model of the ciliary axoneme needs to be constructed to elucidate the effects of hydrodynamics on the ciliary waveform.
3. It is necessary to develop a multiscale analysis method to solve the macroscopic suspension behavior based on the behavior of individual microorganisms. Such a method will help us understand the macroscopic phenomena that often arise in engineering and medicine.
4. Fluid dynamics of ciliary swimming is expected to contribute to microrobot propulsion, mixing, and transport technologies.



DISCLOSURE STATEMENT

The author is not aware of any biases that might be perceived as affecting the objectivity of this review.

ACKNOWLEDGMENTS

I give special acknowledgment to my colleagues Toshihiro Omori and Kenji Kikuchi, current and former students who conducted many of the studies reviewed here. I sincerely thank Timothy J. Pedley for introducing me to the squirmer and for continuing to encourage me. I also thank my collaborators Raymond E. Goldstein, Eric Lauga, Masatoshi Ichikawa, Kenta Ishimoto, and Keiko Numayama-Tsuruta for their interest, support, and enlightening discussions. This research is partly supported by the Japan Society for the Promotion of Science Grant-in-Aid for Scientific Research (JSPS KAKENHI grants 21H04999 and 21H05308).

LITERATURE CITED

- Alert R, Casademunt J, Joanny J-F. 2022. Active turbulence. *Annu. Rev. Condens. Matter Phys.* 13:143–70
- Aragones JL, Yazdi S, Alexander-Katz A. 2018. Diffusion of self-propelled particles in complex media. *Phys. Rev. Fluids* 3:083301
- Batchelor GK. 1970. The stress system in a suspension of force-free particles. *J. Fluid Mech.* 41:545–70
- Bees MA. 2020. Advances in bioconvection. *Annu. Rev. Fluid Mech.* 52:449–76
- Berg HC. 2004. *E. coli in Motion*. New York: Springer-Verlag
- Blake JR. 1971. A spherical envelope approach to ciliary propulsion. *J. Fluid Mech.* 46:199–208
- Böddeker TJ, Karpitschka S, Kreis CT, Magdalaine Q, Bäumchen O. 2020. Dynamic force measurements on swimming *Chlamydomonas* cells using micropipette force sensors. *J. R. Soc. Interface* 17:20190580
- Brennen C, Winet H. 1977. Fluid mechanics of propulsion by cilia and flagella. *Annu. Rev. Fluid Mech.* 9:339–98
- Brumley DR, Pedley TJ. 2019. Stability of arrays of bottom-heavy spherical squirmers. *Phys. Rev. Fluids* 4:053102
- Brumley DR, Polin M, Pedley TJ, Goldstein RE. 2012. Hydrodynamic synchronization and metachronal waves on the surface of the colonial alga *Volvox carteri*. *Phys. Rev. Lett.* 109:268102
- Brumley DR, Polin M, Pedley TJ, Goldstein RE. 2015. Metachronal waves in the flagellar beating of *Volvox* and their hydrodynamic origin. *J. R. Soc. Interface* 12:20141358
- Brumley DR, Wan KY, Polin M, Goldstein RE. 2014. Flagellar synchronization through direct hydrodynamic interactions. *eLife* 3:e02750
- Chamolly A, Ishikawa T, Lauga E. 2017. Active particles in periodic lattices. *New J. Phys.* 19:115001
- Choudhary A, Stark H. 2022. On the cross-streamline lift of microswimmers in viscoelastic flows. *Soft Matter* 18:48–52
- Clopés J, Gompper G, Winkler RG. 2020. Hydrodynamic interactions in squirmer dumbbells: active stress-induced alignment and locomotion. *Soft Matter* 16:10676–87
- Clopés J, Gompper G, Winkler RG. 2022. Alignment and propulsion of squirmer pusher-puller dumbbells. *J. Chem. Phys.* 156:194901
- Corato MD, D'Avino G. 2017. Dynamics of a microorganism in a sheared viscoelastic liquid. *Soft Matter* 13:196–211
- Darveniza C, Ishikawa T, Pedley TJ, Brumley DR. 2022. Pairwise scattering and bound states of spherical microorganisms. *Phys. Rev. Fluids* 7:013104
- Datt C, Elfring GJ. 2019. Active particles in viscosity gradients. *Phys. Rev. Lett.* 123:158006
- Datt C, Zhu L, Elfring GJ, Pak OS. 2015. Squirming through shear-thinning fluids. *J. Fluid Mech.* 784:R1
- Delfau J-B, Molina J, Sano M. 2016. Collective behavior of strongly confined suspensions of squirmers. *Europhys. Lett.* 114:24001
- Dey R, Buness CM, Hokmabad BV, Jin C, Maass CC. 2022. Oscillatory rheotaxis of artificial swimmers in microchannels. *Nat. Commun.* 13:2952



- Dhar A, Burada PS, Sekhar GPR. 2020. Hydrodynamics of active particles confined in a periodically tapered channel. *Phys. Fluids* 32:102005
- Doostmohammadi A, Stocker R, Ardekani AM. 2012. Low-Reynolds-number swimming at pycnoclines. *PNAS* 109:3856–61
- Drescher K, Goldstein RE, Michel N, Polin M, Tuval I. 2010a. Direct measurement of the flow field around swimming microorganisms. *Phys. Rev. Lett.* 105:168101
- Drescher K, Goldstein RE, Tuval I. 2010b. Fidelity of adaptive phototaxis. *PNAS* 107:11171–76
- Drescher K, Leptos K, Tuval I, Ishikawa T, Pedley TJ, Goldstein RE. 2009. Dancing *Volvox*: hydrodynamic bound states of swimming algae. *Phys. Rev. Lett.* 102:168101
- Durham WM, Kessler JO, Stocker R. 2009. Disruption of vertical motility by shear triggers formation of thin phytoplankton layers. *Science* 323:1067–70
- Echigoya S, Sato K, Kishida O, Nakagaki T, Nishigami Y. 2022. Switching of behavioral modes and their modulation by a geometrical cue in the ciliate *Stentor coeruleus*. *Front. Cell Dev. Biol.* 10:1021469
- Elgeti J, Gompper G. 2013. Emergence of metachronal waves in cilia arrays. *PNAS* 110:4470–75
- Evans AA, Ishikawa T, Yamaguchi T, Lauga E. 2011. Orientational order in concentrated suspensions of spherical microswimmers. *Phys. Fluids* 23:111702
- Farutin A, Rafai S, Dysthe DK, Duperray A, Peyla P, Misbah C. 2013. Amoeboid swimming: a generic self-propulsion of cells in fluids by means of membrane deformations. *Phys. Rev. Lett.* 111:228102
- Ferracci J, Ueno H, Numayama-Tsuruta K, Imai Y, Yamaguchi T, Ishikawa T. 2013. Entrapment of ciliates at the water-air interface. *PLOS ONE* 8:e75238
- Fisch C, Dupuis-Williams P. 2011. Ultrastructure of cilia and flagella – back to the future! *Biol. Cell* 103:249–70
- Friedrich BM, Julicher F. 2012. Flagellar synchronization independent of hydrodynamic interactions. *Phys. Rev. Lett.* 109:138102
- Ghose S, Adhikari R. 2014. Irreducible representations of oscillatory and swirling flows in active soft matter. *Phys. Rev. Lett.* 112:118102
- Gidituri H, Shen Z, Würger A, Lintuvuori JS. 2022. Reorientation dynamics of microswimmers at fluid-fluid interfaces. *Phys. Rev. Fluids* 7:L042001
- Gilpin W, Bull MS, Prakash M. 2020. The multiscale physics of cilia and flagella. *Nat. Rev. Phys.* 2:74–88
- Goldstein RE. 2015. Green algae as model organisms for biological fluid dynamics. *Annu. Rev. Fluid Mech.* 47:343–75
- Guasto JS, Rusconi R, Stocker R. 2012. Fluid mechanics of planktonic microorganisms. *Annu. Rev. Fluid Mech.* 44:373–400
- Hamel A, Fisch C, Combettes L, Dupuis-Williams P, Baroud CN. 2011. Transitions between three swimming gaits in *Paramecium* escape. *PNAS* 108:7290–95
- Hausmann K, Allen RD. 2010. Electron microscopy of *Paramecium* (Ciliata). *Methods Cell Biol.* 96:143–73
- Herminghaus S, Maass CC, Kruger C, Thutupalli S, Goehring L, Bahr C. 2014. Interfacial mechanisms in active emulsions. *Soft Matter* 10:7008–22
- Hill NA, Pedley TJ. 2005. Bioconvection. *Fluid Dyn. Res.* 37:1–20
- Huang Z, Omori T, Ishikawa T. 2020. Active droplet driven by a collective motion of enclosed microswimmers. *Phys. Rev. E* 102:022603
- Ingraham JL, Ingraham CA. 2003. *Introduction to Microbiology: A Case-History Approach*. Pacific Grove, CA: Brooks/Cole
- Ishikawa T. 2009. Suspension biomechanics of swimming microbes. *J. R. Soc. Interface* 6:815–34
- Ishikawa T. 2012. Vertical dispersion of model microorganisms in horizontal shear flow. *J. Fluid Mech.* 705:98–119
- Ishikawa T. 2019a. Stability of a dumbbell micro-swimmer. *Micromachines* 10:33
- Ishikawa T. 2019b. Swimming of ciliates under geometric constraints. *J. Appl. Phys.* 125:200901
- Ishikawa T. 2022. Lubrication theory and boundary element hybrid method for calculating hydrodynamic forces between particles in near contact. *J. Comp. Phys.* 452:110913
- Ishikawa T, Brumley DR, Pedley TJ. 2021a. Rheology of a concentrated suspension of spherical squirmers: monolayer in simple shear flow. *J. Fluid Mech.* 914:A26
- Ishikawa T, Dang TN, Lauga E. 2022. Instability of a jet of active fluid. *Phys. Rev. Fluids* 7:093102



- Ishikawa T, Hota M. 2006. Interaction of two swimming *Paramecia*. *J. Exp. Biol.* 209:4452–63
- Ishikawa T, Kikuchi K. 2018. Biomechanics of *Tetrahymena* escaping from a dead end. *Proc. R. Soc. B* 285:20172368
- Ishikawa T, Locsei JT, Pedley TJ. 2008. Development of coherent structures in concentrated suspensions of swimming model micro-organisms. *J. Fluid Mech.* 615:401–31
- Ishikawa T, Locsei JT, Pedley TJ. 2010. Fluid particle diffusion in a semidilute suspension of model micro-organisms. *Phys. Rev. E* 82:021408
- Ishikawa T, Pedley TJ. 2007a. Diffusion of swimming model micro-organisms in a semi-dilute suspension. *J. Fluid Mech.* 588:437–62
- Ishikawa T, Pedley TJ. 2007b. The rheology of a semi-dilute suspension of swimming model micro-organisms. *J. Fluid Mech.* 588:399–435
- Ishikawa T, Pedley TJ. 2008. Coherent structures in monolayers of swimming particles. *Phys. Rev. Lett.* 100:088103
- Ishikawa T, Pedley TJ, Drescher K, Goldstein RE. 2020. Stability of dancing *Volvox*. *J. Fluid Mech.* 903:A11
- Ishikawa T, Simmonds MP, Pedley TJ. 2006. Hydrodynamic interaction of two swimming model micro-organisms. *J. Fluid Mech.* 568:119–60
- Ishikawa T, Tanaka T, Imai Y, Omori T, Matsunaga D. 2016. Deformation of a micro torque swimmer. *Proc. R. Soc. A* 472:20150604
- Ishikawa T, Ueno H, Omori T, Kikuchi K. 2021b. Cilia and centrosomes: ultrastructural and mechanical perspectives. *Semin. Cell Dev. Biol.* 110:61–69
- Ishimoto K. 2017. Guidance of microswimmers by wall and flow: thigmotaxis and rheotaxis of unsteady squirmers in two and three dimensions. *Phys. Rev. E* 96:043103
- Ishimoto K, Gadélha H, Gaffney EA, Smith DJ, Kirkman-Brown J. 2017. Coarse-graining the fluid flow around a human sperm. *Phys. Rev. Lett.* 118:124501
- Ishimoto K, Gaffney EA. 2013. Squirmer dynamics near a boundary. *Phys. Rev. E* 88:062702
- Ito H, Omori T, Ishikawa T. 2019. Swimming mediated by ciliary beating: comparison with a squirmer model. *J. Fluid Mech.* 874:774–96
- Jabbarzadeh M, Fu HC. 2018. Viscous constraints on microorganism approach and interaction. *J. Fluid Mech.* 851:715–38
- Jahn TL, Votta JJ. 1972. Locomotion of protozoa. *Annu. Rev. Fluid Mech.* 4:93–116
- Jibuti L, Qi L, Misbah C, Zimmermann W, Rafai S, Peyla P. 2014. Self-focusing and jet instability of a microswimmer suspension. *Phys. Rev. E* 90:063019
- Kage A, Omori T, Kikuchi K, Ishikawa T. 2020. The shape effect of flagella is more important than bottom-heaviness on passive gravitactic orientation in *Chlamydomonas reinhardtii*. *J. Exp. Biol.* 223:jeb205989
- Kantsler V, Dunkel J, Blayney M, Goldstein RE. 2014. Rheotaxis facilitates upstream navigation of mammalian sperm cells. *eLife* 3:e02403
- Keller SR, Wu TY. 1977. A porous prolate-spheroidal model for ciliated micro-organisms. *J. Fluid Mech.* 80:259–78
- Keller SR, Wu TY, Brennen C. 1975. A traction-layer model for ciliary propulsion. In *Swimming and Flying in Nature*, ed. TY Wu, C Brennen, CJ Brokaw, pp. 253–72. New York: Plenum Press
- Kessler JO. 1986. Individual and collective dynamics of swimming cells. *J. Fluid Mech.* 173:191–205
- Khan S, Scholey JM. 2018. Assembly, functions and evolution of archaella, flagella and cilia. *Curr. Biol.* 28:R278–92
- Kim S, Karrila SJ. 1991. *Microhydrodynamics: Principles and Selected Applications*. Boston: Butterworth Heinemann
- Kirk DL. 1998. *Volvox: Molecular-Genetic Origins of Multicellularity and Cellular Differentiation*. Cambridge, UK: Cambridge Univ. Press
- Koch DL, Subramanian G. 2011. Collective hydrodynamics of swimming microorganisms: living fluids. *Annu. Rev. Fluid Mech.* 43:637–59
- Kogure Y, Omori T, Ishikawa T. 2023. Flow-induced diffusion in a packed lattice of squirmers. *J. Fluid Mech.* In press
- Kree R, Burada PS, Zippelius A. 2017. From active stresses and forces to self-propulsion of droplets. *J. Fluid Mech.* 821:595–623



- Kree R, Rückert L, Zippelius A. 2021. Dynamics of a droplet driven by an internal active device. *Phys. Rev. Fluids* 6:034201
- Kunita I, Yamaguchi T, Tero A, Akiyama M, Kuroda S, Nakagaki T. 2016. A ciliate memorizes the geometry of a swimming arena. *J. R. Soc. Interface* 13:20160155
- Kyoya K, Matsunaga D, Imai Y, Omori T, Ishikawa T. 2015. Shape matters: Near-field fluid mechanics dominate the collective motions of ellipsoidal squirmers. *Phys. Rev. E* 92:063027
- Lauga E. 2016. Bacterial hydrodynamics. *Annu. Rev. Fluid Mech.* 48:105–30
- Lauga E, Powers TR. 2009. The hydrodynamics of swimming microorganisms. *Rep. Prog. Phys.* 72:096601
- Leptos KC, Guasto JS, Gollub JP, Pesci AI, Goldstein RE. 2009. Dynamics of enhanced tracer diffusion in suspensions of swimming eukaryotic microorganisms. *Phys. Rev. Lett.* 103:198103
- Li G, Ardekani AM. 2014. Hydrodynamic interaction of microswimmers near a wall. *Phys. Rev. E* 90:013010
- Li G, Ostace A, Ardekani AM. 2016. Hydrodynamic interaction of swimming organisms in an inertial regime. *Phys. Rev. E* 94:053104
- Lighthill MJ. 1952. On the squirming motion of nearly spherical deformable bodies through liquids at very small Reynolds numbers. *Commun. Pure Appl. Math.* 5:109–18
- Lintuvuori JS, Würger A, Stratford K. 2017. Hydrodynamics defines the stable swimming direction of spherical squirmers in a nematic liquid crystal. *Phys. Rev. Lett.* 119:068001
- Maleprade H, Moisy F, Ishikawa T, Goldstein RE. 2020. Motility and phototaxis of *Gonium*, the simplest differentiated colonial alga. *Phys. Rev. E* 101:022416
- Manabe J, Omori T, Ishikawa T. 2020. Shape matters: entrapment of a model ciliate at interfaces. *J. Fluid Mech.* 892:A15
- Marcos Fu HC, Powers TR, Stocker R. 2012. Bacterial rheotaxis. *PNAS* 109:4780–85
- Matsui H, Omori T, Ishikawa T. 2020a. Hydrodynamic interaction of two deformable torque swimmers. *J. Fluid Mech.* 894:A9
- Matsui H, Omori T, Ishikawa T. 2020b. Rheology of a dilute suspension of deformable microswimmers. *Phys. Fluids* 32:071902
- Milana E, Zhang R, Vetrano MR, Peerlinck S, de Volder M, et al. 2020. Metachronal patterns in artificial cilia for low Reynolds number fluid propulsion. *Sci. Adv.* 6:eabd2508
- Modica KJ, Xi Y, Takatori SC. 2022. Porous media microstructure determines the diffusion of active matter: experiments and simulations. *Front. Phys.* 10:869175
- Moran JL, Posner JD. 2017. Phoretic self-propulsion. *Annu. Rev. Fluid Mech.* 49:511–40
- More RV, Ardekani AM. 2021. Hydrodynamic interactions between swimming microorganisms in a linearly density stratified fluid. *Phys. Rev. E* 103:013109
- Moreau C, Ishimoto K. 2021. Driving a microswimmer with wall-induced flow. *Micromachines* 12:1025
- Morita T, Omori T, Ishikawa T. 2018. Biaxial fluid oscillations can propel a micro-capsule swimmer in an arbitrary direction. *Phys. Rev. E* 98:063102
- Nagai K, Sumino Y, Kitahata H, Yoshikawa K. 2005. Mode selection in the spontaneous motion of an alcohol droplet. *Phys. Rev. E* 71:065301(R)
- Naitoh Y, Eckert R. 1969. Ionic mechanisms controlling behavioral responses of *Paramecium* to mechanical stimulation. *Science* 164:963–65
- Narematsu N, Quek R, Chiam K-H, Iwadate Y. 2015. Ciliary metachronal wave propagation on the compliant surface of *Paramecium* cells. *Cytoskeleton* 72:633–46
- Nganguia H, Pietrzak K, Pak OS. 2017. Swimming efficiency in a shear-thinning fluid. *Phys. Rev. E* 96:062606
- Nishigami Y, Ohmura T, Taniguchi A, Nonaka S, Manabe J, et al. 2018. Influence of cellular shape on sliding behavior of ciliates. *Commun. Integr. Biol.* 11:e1506666
- Ohmura T, Nishigami Y, Taniguchi A, Nonaka S, Ishikawa T, Ichikawa M. 2021. Near-wall rheotaxis of the ciliate *Tetrahymena* induced by the kinesthetic sensing of cilia. *Sci. Adv.* 7:eaibi5878
- Ohmura T, Nishigami Y, Taniguchi A, Nonaka S, Manabe J, et al. 2018. Simple mechanosense and response of cilia motion reveal the intrinsic habits of ciliates. *PNAS* 115:3231–36
- Okuyama K, Nishigami Y, Ohmura T, Ichikawa M. 2021. Accumulation of *Tetrahymena pyriformis* on interfaces. *Micromachines* 12:1339
- Omori T, Ito H, Ishikawa T. 2020. Swimming microorganisms acquire optimal efficiency with multiple cilia. *PNAS* 117:30201–7



- Omori T, Kikuchi K, Schmitz M, Pavlovic M, Chuang C-H, Ishikawa T. 2022. Rheotaxis and migration of an unsteady microswimmer. *J. Fluid Mech.* 930:A30
- Ortlib L, Rafaï S, Peyla P, Wagner C, John T. 2019. Statistics of colloidal suspensions stirred by microswimmers. *Phys. Rev. Lett.* 122:148101
- Osterman N, Vilfan A. 2011. Finding the ciliary beating pattern with optimal efficiency. *PNAS* 108:15727–32
- Ouillon R, Houghton IA, Dabiri JO, Meiburg E. 2020. Active swimmers interacting with stratified fluids during collective vertical migration. *J. Fluid Mech.* 902:A23
- Ouyang Z, Lin J. 2021. The hydrodynamics of an inertial squirmer rod. *Phys. Fluids* 33:073302
- Ouyang Z, Lin J, Phan-Thien N. 2022a. Swimming of an inertial squirmer array in a Newtonian fluid. *Phys. Fluids* 34:053303
- Ouyang Z, Lin Z, Yu Z, Lin J, Phan-Thien N. 2022b. Hydrodynamics of an inertial squirmer and squirmer dumbbell in a tube. *J. Fluid Mech.* 939:A32
- Oyama N, Molina JJ, Yamamoto R. 2016. Purely hydrodynamic origin for swarming of swimming particles. *Phys. Rev. E* 93:043114
- Papavassiliou D, Alexander GP. 2017. Exact solutions for hydrodynamic interactions of two squirming spheres. *J. Fluid Mech.* 813:618–46
- Pedley TJ. 2016. Spherical squirmers: models for swimming micro-organisms. *IMA J. Appl. Math.* 81:488–521
- Pedley TJ, Brumley DR, Goldstein RE. 2016. Squirmers with swirl: a model for *Volvox* swimming. *J. Fluid Mech.* 798:165–86
- Pedley TJ, Kessler JO. 1992. Hydrodynamic phenomena in suspensions of swimming microorganisms. *Annu. Rev. Fluid Mech.* 24:313–58
- Persat A, Nadell CD, Kim MK, Ingremeau F, Siryaporn A, et al. 2015. The mechanical world of bacteria. *Cell* 161:988–97
- Poddar A, Bandopadhyay A, Chakraborty S. 2020. Near-wall hydrodynamic slip triggers swimming state transition of micro-organisms. *J. Fluid Mech.* 894:A11
- Potomkin M, Gyrya V, Aranson I, Berlyand L. 2013. Collision of microswimmers in a viscous fluid. *Phys. Rev. E* 87:053005
- Purcell EM. 1977. Life at low Reynolds number. *Am. J. Phys.* 45:3–11
- Qi K, Anepu H, Gompper G, Winkler RG. 2020a. Rheotaxis of spheroidal squirmers in microchannel flow: interplay of shape, hydrodynamics, active stress, and thermal fluctuations. *Phys. Rev. Res.* 2:033275
- Qi K, Westphal E, Gompper G, Winkler RG. 2020b. Enhanced rotational motion of spherical squirmer in polymer solutions. *Phys. Rev. Lett.* 124:068001
- Qiu T, Lee T-C, Mark AG, Morozov KI, Münster R, et al. 2014. Swimming by reciprocal motion at low Reynolds number. *Nat. Commun.* 5:5119
- Raina J-B, Fernandez V, Lambert B, Stocker R, Seymour JR. 2019. The role of microbial motility and chemotaxis in symbiosis. *Nat. Rev. Microbiol.* 17:284–94
- Roberts AM, Deacon FM. 2002. Gravitaxis in motile micro-organisms: the role of fore-aft body asymmetry. *J. Fluid Mech.* 452:405–23
- Rode S, Elgeti J, Gompper G. 2021. Multi-ciliated microswimmers–metachronal coordination and helical swimming. *Eur. Phys. J. E* 44:76
- Rühle F, Stark H. 2020. Emergent collective dynamics of bottom-heavy squirmers under gravity. *Eur. Phys. J. E* 43:26
- Saintillan D. 2018. Rheology of active fluids. *Annu. Rev. Fluid Mech.* 50:563–92
- Schaar K, Zöttl A, Stark H. 2015. Detention times of microswimmers close to surfaces: influence of hydrodynamic interactions and noise. *Phys. Rev. Lett.* 115:038101
- Seemann R, Fleury J-B, Maass CC. 2016. Self-propelled droplets. *Eur. Phys. J.* 225:2227–40
- Shaik VA, Ardekani AM. 2017. Motion of a model swimmer near a weakly deforming interface. *J. Fluid Mech.* 824:42–73
- Shaik VA, Ardekani AM. 2021. Squirming in density-stratified fluids. *Phys. Fluids* 33:101903
- Shaik VA, Elfring GJ. 2021. Hydrodynamics of active particles in viscosity gradients. *Phys. Rev. Fluids* 6:103103
- Shen Z, Lintuvuori JS. 2019. Gravity induced formation of spinners and polar order of spherical microswimmers on a surface. *Phys. Rev. Fluids* 4:123101



- Shikata T, Matsunaga S, Nishide H, Sakamoto S, Onistuka G, Yamaguchi M. 2015. Diurnal vertical migration rhythms and their photoresponse in four phytoflagellates causing harmful algal blooms. *Limnol. Oceanogr.* 60:1251–64
- Short MB, Solari CA, Ganguly S, Powers TR, Kessler JO, Goldstein RE. 2006. Flows driven by flagella of multicellular organisms enhance long-range molecular transport. *PNAS* 103:8315–19
- Simmchen J, Katuri J, Uspal WE, Popescu MN, Tasinkevych M, Sanchez S. 2016. Topographical pathways guide chemical microswimmers. *Nat. Commun.* 7:10598
- Sleigh MA. 1962. *The Biology of Cilia and Flagella*. Oxford, UK: Pergamon Press
- Soni H, Pelcovits RA, Powers TR. 2018. Enhancement of microorganism swimming speed in active matter. *Phys. Rev. Lett.* 121:178002
- Spagnolie SE, Lauga E. 2012. Hydrodynamics of self-propulsion near a boundary: predictions and accuracy of far-field approximations. *J. Fluid Mech.* 700:105–47
- Tarama M. 2017. Dynamics of deformable active particles under external flow field. *J. Phys. Soc. Jpn.* 86:101011
- Theers M, Westphal E, Gompper G, Winkler RG. 2016. Modeling a spheroidal microswimmer and cooperative swimming in a narrow slit. *Soft Matter* 12:7372–85
- Theers M, Westphal E, Winkler RG, Gompper G. 2018. Clustering of microswimmers: interplay of shape and hydrodynamics. *Soft Matter* 14:8590–603
- Thiffeault J-L. 2015. Distribution of particle displacements due to swimming microorganisms. *Phys. Rev. E* 92:023023
- Thutupalli S, Seemann R, Herminghaus S. 2011. Swarming behavior of simple model squirmers. *New J. Phys.* 13:073021
- Uspal WE, Popescu MN, Dietrich S, Tasinkevych M. 2015. Rheotaxis of spherical active particles near a planar wall. *Soft Matter* 11:6613–32
- van Gogh B, Demir E, Palaniappan D, Pak OS. 2022. The effect of particle geometry on squirming through a shear-thinning fluid. *J. Fluid Mech.* 938:A3
- Walker BJ, Ishimoto K, Moreau C, Gaffney EA, Dalwadi MP. 2022. Emergent rheotaxis of shape-changing swimmers in Poiseuille flow. *J. Fluid Mech.* 944:R2
- Wan KY, Goldstein RE. 2016. Coordinated beating of algal flagella is mediated by basal coupling. *PNAS* 113:E2784–93
- Wang L, Meng Z, Chen Y, Zheng Y. 2021. Engineering magnetic micro/nanorobots for versatile biomedical applications. *Adv. Intell. Syst.* 3:2000267
- Wang S, Ardekani AM. 2015. Biogenic mixing induced by intermediate Reynolds number swimming in stratified fluids. *Sci. Rep.* 5:17448
- Wang W, Duan W, Ahmed S, Sen A, Mallouk TE. 2015. From one to many: dynamic assembly and collective behavior of self-propelled colloidal motors. *Acc. Chem. Res.* 48:1938–46
- Wang W, Liu Q, Tanasijevic I, Reynolds MF, Cortese AJ, et al. 2022. Cilia metasurfaces for electronically programmable microfluidic manipulation. *Nature* 605:681–86
- Westwood TA, Keaveny EE. 2021. Coordinated motion of active filaments on spherical surfaces. *Phys. Rev. Fluids* 6:L121101
- Yoshinaga N, Liverpool TB. 2017. Hydrodynamic interactions in dense active suspensions: from polar order to dynamical clusters. *Phys. Rev. E* 96:020603(R)
- Yoshinaga N, Liverpool TB. 2018. From hydrodynamic lubrication to many-body interactions in dense suspensions of active swimmers. *Eur. Phys. J. E* 41:76
- Zantop AW, Stark H. 2022. Emergent collective dynamics of pusher and puller squirmers rods: swarming, clustering, and turbulence. *Soft Matter* 18:6179–91
- Zhu L, Lauga E, Brandt L. 2012. Self-propulsion in viscoelastic fluids: pushers versus pullers. *Phys. Fluids* 24:051902
- Zöttl A, Stark H. 2012. Nonlinear dynamics of a microswimmer in Poiseuille flow. *Phys. Rev. Lett.* 108:218104
- Zöttl A, Stark H. 2014. Hydrodynamics determines collective motion and phase behavior of active colloids in quasi-two-dimensional confinement. *Phys. Rev. Lett.* 112:118101
- Zöttl A, Stark H. 2016. Emergent behavior in active colloids. *J. Phys. Condens. Matter* 28:253001

